UNIVERSITÄTSKLINIKUM HAMBURG-EPPENDORF

Labor „Experimental Research in Stroke and Inflammation“ (ERSI)
Klinik und Poliklinik für Neurologie

Prof. Tim Magnus // Prof. Götz Thomalla

Purinergic signaling in CD8 T cells and endothelial cells during experimental murine cerebral vasculitis

Dissertation

zur Erlangung des Grades eines Doktors der Medizin
an der Medizinischen Fakultät der Universität Hamburg.

vorgelegt von:

Alexander Veltkamp
Aus Winston-Salem (North-Carolina, USA)

Hamburg 2024

Angenommen von der
Medizinischen Fakultät der Universität Hamburg am: 27.06.2025

Veröffentlicht mit Genehmigung der
Medizinischen Fakultät der Universität Hamburg.

Prüfungsausschuss, der/die Vorsitzende: Prof. Dr. Hans-Willi Mittrücker

Prüfungsausschuss, zweite/r Gutachter/in: Prof. Dr. Tim Magnus

Table of contents

1. Introduction

1.1 Purinergic signaling

Purine nucleotides such as adenosine triphosphate (ATP) are well known as intracellular energy carriers, maintaining basic cellular functions, proliferation, or cell motility. In addition to their intracellular role, purine nucleotides also act as extracellular co-transmitters. In 1972, Geoffrey Burnstock reported that inhibitory nerves supplying smooth-muscle cells in guinea pig taenia coli exhibited an electrical hyperpolarizing activity that could only be attributed to purine nucleotides (Burnstock, 1972). He coined the term “purinergic signaling” and was denounced for about two decades for his hypothesis of extracellular purinergic transmitters.

However, since the 1990s it has been possible to clone the receptors for adenosine triphosphate (ATP), adenosine, and other purine nucleotides. Purinergic signaling plays an important role in peripheral and central neurons (Burnstock, 2007), in pain nociception (Tsuda et al., 2010) and as a regulatory system for blood pressure (Burnstock and Ralevic, 1994). In addition, therapeutic modulation of purinergic signaling has been evaluated in a wide range of diseases such as supraventricular tachycardia, Parkinson’s disease, thrombosis, chronic cough, bladder incontinence, visceral pain, and hypertension (Burnstock, 2017). Great potential for research into purinergic signaling is particularly seen in the field of immunology, and pharmacological agents such as P2X7 antagonists appear promising (Burnstock and Knight, 2018).

1.2 Danger associated molecular patterns (DAMPS)

A fundamental principle of immunology is that the immune system discriminates between ‘self’ and ‘non self’. In 1989, Charles Janeway postulated that innate immune cells express genetically encoded pattern recognition receptors (PRRs), that can recognize pathogen-associated molecular patterns (PAMPs) such as lipopolysaccharides on bacteria (Janeway, 1992). However, inflammation can also occur sterile in the absence of microorganisms. Sterile inflammation typically stems from the recognition of intracellular contents released from damaged cells, which are called danger-associated molecular patterns (DAMPs) (Chen and Nunez, 2010). DAMPs and PAMPs can trigger immune responses by activating

classical pattern recognition receptors (e.g. Toll-like receptors, NOD-like receptors). Further non-pattern recognition receptors (e.g. RAGE, GPCRs and ion channels) are involved in the recognition of danger molecules (Gong et al., 2020).

An important example for ubiquitous DAMPs are extracellular purine nucleotides such as ATP that promote an immune response via specific purinergic receptors (Yuan et al., 2021).

1.3 ATP signaling via the P2X7 receptor

During sterile inflammation ATP accumulates locally through disrupted cell membranes or membrane proteins (Linden et al., 2019). ATP is then sensed by all ionotropic P2X channels and some metabotropic P2Y receptors. Interestingly, the P2X7 receptor stands out with high expression and unique biochemical features in various immune cells such as innate myeloid phagocytes and T cells (McCarthy et al., 2019).

A major effect of the P2X7 pathway in innate myeloid phagocytes is the activation of the multiprotein NLRP3 inflammasome with subsequent interleukin-1 beta release (Pelegrin, 2021). The NLRP3-P2X7 axis is currently under clinical investigation for the treatment of different inflammatory, metabolic, and neurodegenerative diseases (Pelegrin, 2021).

In T cells the P2X7 pathway contributes to activation, subclass differentiation and migration to secondary lymphoid organs (Vultaggio-Poma and Di Virgilio, 2022, Grassi, 2020). However, prolonged activation of P2X7 and higher micromolar concentrations of ATP can also induce cell death (Di Virgilio et al., 2017). In mice, P2X7 mediated cell death can also be mediated via nicotinamide adenine dinucleotide (NAD) dependent ADP-ribosylation of the P2X7 receptor through ARTC2 (Seman et al., 2003, Rissiek et al., 2018). Beyond that, the P2X7 pathway activates the metalloproteases ADAM10 and ADAM17, which catalyze the shedding of surface molecules such as CD62L, CD27 and IL-6R on T cells (Grassi, 2020). Intriguingly, the P2X7 pathway promotes mitochondrial homeostasis and is required for the selective survival of tissue-resident memory CD8 T cells (Borges da Silva et al., 2020).

In contrast to this physiological role in CD8 T cells, tissue-resident CD8 T cells in the liver can become auto-aggressive against hepatocytes after MHC-independent activation via P2X7 in non-alcoholic steatohepatitis (NASH) (Dudek et al., 2021). Interestingly, inhibition of P2X7 prevented CD8 T cell auto-aggression but preserved the antigen-specific cytotoxicity of CD8 T cells (Dudek et al., 2021). Taken together, the P2X7 pathway has a dual role in T cells either supporting T cell functions or killing them depending on the duration, magnitude, and context of the P2X7 activation.

1.4 Conversion of extracellular ATP to adenosine by ecto-enzymes

Extracellular adenosine is generated by the degradation of ATP to adenosine monophosphate (AMP) by the ectoenzymes CD39 and further to adenosine by CD73 (Giuliani et al., 2020). Adenosine signaling can have anti-inflammatory effects in disease settings such as inflammation of bowel or lung, and in the immunosuppressive tumor microenvironment (Vuerich et al., 2020, Li et al., 2020, Steingold and Hatfield, 2020). In line with that, studies have shown that the A2 receptor for adenosine is required for proper limitation and termination of inflammation in various mouse models (Ohta and Sitkovsky, 2001).

T cells express only the A2a receptor that can limit T cell differentiation and metabolic fitness in concert with CD73 (Cekic and Linden, 2016).

In accordance with that, CD73 can reduce the CD8 T cell survival following an antigenic stimulus while promoting survival during homeostasis (Rosemblatt et al., 2021). Thus, CD73 and CD39 serve as inhibitory immune checkpoint molecules with a tissue dependent functional impact (Smith and Snyder, 2021, Allard et al., 2017).

To unravel the functional impact of adenosine signaling and its associated ecto-enzymes, various pharmacological agents can be used such as small molecule inhibitors, antibodies or newly developed nanobodies (Menzel et al., 2024).

1.5 Targeting purinergic signaling with nanobodies

Nanobodies are single-domain immunoglobulin (Ig) fragments derived from naturally occurring heavy chain antibodies of camelids, such as llamas and alpacas (Eggers et al., 2021, Muyldermans, 2013). Their unique structure with a

long CDR3 loop in the antigen binding region allows them to reach less accessible epitopes such as the ligand binding site of an ionotropic receptor (Menzel et al., 2018, Lauwereys et al., 1998). Moreover, nanobodies have several pharmacological advantages over antibodies, such as fewer off-target effects, high solubility, increased tissue penetration (e.g. blood-brain-barrier), and greater ability to modulate enzyme function and ion channel activity (Menzel et al., 2018, Danquah et al., 2016). These properties make nanobodies an attractive tool for blocking ion channels such as P2X7 in preclinical animal models.

A specific inhibitory nanobody (13A7) was developed to block ATP- and NAD-induced gating of the P2X7 receptor on murine T cells and macrophages (Danquah et al., 2016, Pinto, 2018). By this, 13A7 nanobody blockade prevents ATP/NAD-mediated shedding of CD27 shedding on spleen derived T cells.

Therapeutic application of the P2X7-blocking nanobody 13A7 *in vivo* ameliorated inflammation in mouse models of experimental glomerulonephritis and allergic contact dermatitis (Danquah et al., 2016). This effect was evident in both the sensitization and challenge phases of the T cell based allergic contact dermatitis model suggesting that multiple P2X7 expressing immune subsets were involved. As T cells are fundamental to the pathology of many autoimmune diseases, future preclinical mouse studies may reveal the contribution of P2X7 in other inflammatory mouse models. As nanobodies can cross the blood-brain-barrier much easier than large monoclonal antibodies, P2X7 receptor-targeting nanobodies are also promising agents for the treatment of inflammatory central nervous system disorders (Burnstock, 2017).

1.6 Primary Angiitis of the Central Nervous System (PACNS)

Primary Angiitis of the Central Nervous System (PACNS) is a rare autoinflammatory disease with an incidence of 2.4 cases per million person-years. PACNS usually affects middle-aged adults with a mean age of 51 years. The clinical presentation is nonspecific, and the most common symptoms are cognitive and affective abnormalities, headache, and multifocal symptoms associated with recurrent ischemic or hemorrhagic episodes (Kraemer and Berlit, 2021).

PACNS can cause ischemic strokes or bleedings localized in disseminated vascular beds. The dissemination of these lesions is the reason why even the diagnostic gold standard, brain biopsy, has a high false-negative rate (Berlit and Krämer, 2018). In addition, angiography and MRI can be useful in the diagnosis of PACNS but both lack high sensitivity and specificity. Due to the challenging nature of the diagnosis, important differential diagnoses must be ruled out prior to immunosuppressive treatment. These diagnoses include reversible cerebral vasoconstriction syndrome, cerebral manifestation of systemic vasculitis or rheumatic diseases, Moya-Moya angiopathy and infectious angiopathies (Kraemer and Berlit, 2021).

Histologically, PACNS inflammation can be divided into three subtypes: Granulomatous, Necrotizing, and Lymphocytic (Miller et al., 2009). A combination of these histologic features is also possible, making it even more difficult to distinguish it from other vasculitides. Immunohistochemically, PACNS can be subdivided into granulomatous, non-granulomatous and amyloid beta related PACNS. All PACNS subtypes share the appearance of B cells, CD3 T cells, CD4 helper T cells, CD8 cytotoxic T cells, and macrophages in or around vessels. The frequent involvement of specific lymphocyte populations in PACNS suggests an unknown persistent antigenic trigger.

1.7 Recent development of mouse models for cerebral vasculitis

To date, there is no mouse model for primary CNS angiitis. However, a mouse model was developed in which CD8 T cells attack brain endothelial cells, that is thought to resemble the findings in patients with Susac syndrome (Gross et al., 2019). Susac syndrome is an inflammatory endotheliopathy affecting small to medium sized vessels of the retina, inner ear, and brain. It is characterized by occlusions of small arteries leading to neurological deficits (Gross et al., 2019). Current thinking is that the small artery occlusions have an auto-inflammatory genesis that is antigen-driven and directed against the brain endothelium (Deb-Chatterji et al., 2019). Gross and coworkers found that patients with Susac syndrome have dominantly activated CD8+ T cells in both the peripheral blood and CSF. Terminally differentiated effector memory CD8+ T cells were significantly increased in patients with Susac syndrome, suggesting the presence

of a strong and prolonged antigenic stimulus. These effector memory CD8+ T cells show disease-specific expanded T cell receptor clones with an increased cytolytic potential compared to healthy controls. The authors developed a mouse model of Susac syndrome by crossing Rosa26tm(HA)1Lib with Slco1c1-CreERT2 mice. Slco1c1-CreERT2 mice allow Cre recombinase expression specifically in brain ECs. Tamoxifen treatment for 5 days (i.p.; 1 mg per mouse per day) induces Cre expression in the brain endothelial cells, resulting in activation of the immunogenic hemagglutinin (HA) coding sequence with a leading STOP codon flanked by loxP sites (Gross et al., 2019). This hemagglutinin-based model relies on the adoptive transfer of HA-epitope specific CD8 T cells, but the authors did not evaluate the endogenous anti-HA response. In addition, the HA-antigen could potentially be expressed in the thymus inducing central HA-specific tolerance. This could prevent an endogenous immune response. To allow analyses of an endogenous CD8 T cell response against neoantigens presented by brain endothelial cells, the group of Dr. Rissiek developed a new ovalbumin(OVA)-based mouse model, termed BrEndO mouse. BrEndo stands for Brain Endothelial OVA. Tamoxifen treatment induces OVA-expression in brain endothelial cells, leading to a subsequent anti-OVA CD8 T cell response at the BBB (more information on the BrEndO mouse can be found in section 2.2)

1.8 Objectives of the project

The overall objective of this project was to characterize the role of purinergic signaling in the BrEndO mouse model.

Specific goals for the for this thesis were:

i. to characterize the expression of P2X7 and the ecto-enzymes CD39/CD73 of brain-infiltrating cytotoxic T cells in BrEndO mice.
ii. to evaluate the therapeutic potential of P2X7-blocking nanobodies in BrEndO mice.
iii. to analyze the mRNA sequencing data from isolated brain microvessels of Cre(+) BrEndO and Cre(–) control mice towards the expression of key players in purinergic signaling.
iv. to genetically engineer murine brain endothelial cells (bEnd.3) to express CD73.

2. Material and Methods

2.1 Material tables

Table 1: Laboratory equipment

equipment	model	company
analytical scale	PL602-S	Mettler-Toledo
cell counting chamber	Neubauer CC	Marienfeld-Superior
centrifuge	5430 R	Eppendorf
centrifuge	5810 R	Eppendorf
centrifuge	5804 R	Eppendorf
clicker for cell counting		Infactory
DNA Gel Electrophoresis	Sub-Cell GT	BioRad
flow cytometer	FACSCelesta™	BD Biosciences
	FACSCantoII™	BD Biosciences
	FACS LSR FortessaA3™ Flow Cytometer	BD Biosciences
	FACSAria Illu sorter	BD Biosciences
	FACSAria Fusion sorter	BD Biosciences
freezer	-20℃	Liebherr
	-80℃	Panasonic
fridge	4℃	Liebherr
incubator	MCO-5ACUV	Panasonic
qPCR machine	Light cycler 96	Roche
luminescent machine	Vector 2	Perkin Elmer
metal needle with spoon		Bochem
microscope	Axiovert 40 CFL	ZEISS
microwave		AEG
nanodrop	Nanodrop 2000c	Thermo Scientific
pipetboy		Integra
protein gel electrophoresis	Mini-Cell	Novex
scanner	4990	Epson
scissors	Various (bone, curved etc.)	
shaker incubator	Ecotron	INFORS HT

thermomixer	F1.5	Eppendorf
ultraviolet transilluminator	TFL-35M	Vilber Lourmat
uv-lamp		Kodak
vacuum pump	Laboport	KFN Lab
vibration shaker	Roto-Shake Genie	Scientific Industries
vortex	54113	Heidolph
water bath	GLS400	Grant
	1002	GFL
workbench	Class II Type A/B3	Baker

Table 2: Consumables

material	**type**	**company**
96-well white plate		Nunc
96-well plate for light cycler		
96-well plate		Greiner
12-well plate		Greiner
6-well plate		Greiner
cannula	Sterican, various sizes	Braun
cellulose chromatography paper	Whatman paper	Sigma-Aldrich
cell culture flasks	T25, T75	Greiner
cell strainer	70 µm, 40 µm (for 50 ml and 15 ml falcon tubes)	Greiner
combi tips	various sizes	Eppendorf
FACS tubes	5 ml	SARSTEDT
falcon tube	15 ml, 50 ml	Greiner
gloves	Coated	Ansell
	Nitra-Tex	Ansell
microcentrifuge tubes	various sizes	Eppendorf
parafilm	PM-996	Bemis
pipette tips	various sizes	Eppendorf
	various sizes	Th.Geyer

petri dish	various sizes	Greiner
protective films		Thermo Fisher Scientific
serological pipettes	various sizes	Greiner
syringes	Various sizes	Braun
trucount tubes		BD Biosciences

Table 3: Reagents (kits)

purpose	**name**	**company**
CD73 functional assay	AMP-Glo™ assay Kit	Promega
cytokine kit	LEGENDplex™ Mouse Th17 Panel (8-plex) with Filter Plate V02	Biolegend
dead cell dye	Trypan Blue solution 0.4 %	Sigma-Aldrich Chemie GmbH, München
fluorescent calcium	Fluo4 AM, cell permeant	Thermo Fisher Scientific
MN DNA purification kit	Macherey-Nagel™ NucleoSpin™ Gel and PCR Clean-up Kit	Thermo Fisher Scientific
		Thermo Fisher Scientific
permanent cell dye	Invitrogen™ eBioscience™ Cell Proliferation Dye eFluor™ 670	Invitrogen
plasmid purification	Miniprep Kit	Qiagen
	Endofree Maxiprep Kit	Qiagen
plasmid ligation	Quick Ligation Kit	NEB
quantitative polymerase chain reaction (qPCR)	Maxima probe qPCR master mix (2x)	Thermo Fisher Scientific
quantitative polymerase chain reaction (qPCR)	Taqman probes	Thermo Fisher Scientific
RNA isolation	RNeasy kit	Qiagen
reducing agent for SDS PAGE	NuPAGE™ reducing agent (10x), 500 mM Dithiothreitol	Thermo Fisher Scientific

	DTT	
SDS PAGE gel	4-12% NuPAGE	Invitrogen
SDS PAGE buffer	NuPAGE™ LDS-Probe buffer (4x)	Thermo Fisher Scientific
sequencing	Mix2Seq Kit	Eurofins

Table 4: Chemicals

chemicals	**company**
Adenosin-5'-triphosphat TP	Sigma
bovine serum albumin, BSA	Sigma
carbenicillin	Gibco
coomassie stain	Bio-Rad
corn oil	Thermo Fisher Scientific
4′,6-Diamidin-2-phenylindol (DAPI)	Thermo Fisher Scientific
DMEM medium	Gibco
Easycoll (L6145)	Biochrome GmbH
EDTA	Sigma
FBS Good Forte	PAN seratech
FreeStyle™ 293 Expression Medium	Gibco
IMDM medium	Gibco
isoflurane	Baxter
JetPEI	Polyplus
kanamycin	Gibco
LB Agar	Invitrogen
LB Broth	Invitrogen
loading Dye, 6x	Thermo Fisher Scientific
magnesium chloride, MgCl2	Sigma
MCDB131 Medium, no glutamine	Thermo Fisher Scientific
NaCl 0.9 %	B. Braun
NuPAGE antioxidant	Invitrogen
NuPAGE sample reducing agent, 10x	Invitrogen
NuPAGE SDS-PAGE sample buffer, 4x	Invitrogen

PBS, 1x	Gibco
Pen/Strep	Gibco
potassium chloride, KCl	Merck
Roti Gel Stain (20,000x concentration)	Roth
sodium chloride, NaCl	Merck
Tris-Acetat-EDTA Puffer (TAE)	Invitrogen
trypsin, 10x	Gibco

Table 5: Mediums

medium	**composition**
bacterial culture medium	
LB-Medium	20 g/l in deionized Water 8 mg in 400ml ddH_2O, autoclave
LB-Agar	32 g/l in deionized Water 12,8 mg in 400ml ddH_2O, autoclave
SOC-Medium	2% (w/v) Tryptone
	0.5% (w/v) Yeast extract
	10 mM NaCl
	2.5 mM KCl
	10 mM $MgCl_2$
	20 mM Glucose
eukaryotic medium	
complete DMEM	DMEM (1x) + GlutaMax
	10% FCS
complete IMDM	IMDM (1x)
	Gentamycin 500 µl (50 µg/ml)
	β-Mercaptoethanol 500 µl (0.1 mM)
feeding medium (for transfected HEK-6e cells)	FreeStyle™ 293 Expression Medium
	20% tryptone

Table 6: Buffers

buffer	composition
ammonium-chloride-potassium (ACK) erythrocyte lysis buffer	155 mM ammonium chloride, 10 mM kalium hydrogen carbonate, 100 mM EDTA, pH 7.2-7.4. Dilute 8.02 g ammonium chloride, 1 g kalium hydrogen carbonate, and 37 mg EDTA in 1 L of ddH20
CutSmart Buffer™ 10X	1X Buffer Components: 50 mM Potassium Acetate, 20 mM Tris-acetate, 10 mM Magnesium Acetate, 100 µg/ml Recombinant Albumin, pH 7.9; Use at 1X concentration 1 µl in 50 µl total volume.
DAPI staining of cell membrane pores	0.15 mM DAPI in PBS stock solution. Use at a final concentration of 1.5 µM
FACS buffer	1 l PBS (1x), 2 g BSA (0.2%), 1 ml EDTA (0.5 mM)
SDS-PAGE gel running buffer (1x)	20x MES buffer diluted in de-ionized water
digestion solution	100 µg/ml DNase I and 1 mg/ml collagenase A in DMEM.
Percoll gradient solution	33% Percoll solution diluted with 1 x PBS stored at 4°C.

Table 7: Antibodies

antigen	fluorochrome	clone	company	dilution
mouse CD3e	BV421	145-2C11	BioLegend	1:100
mouse CD4	BV605	RM 4-5	BioLegend	1:100
mouse CD4	AF700	RM 4-5	BioLegend	1:100
mouse CD8a	BV711	53-6.7	BioLegend	1:100
mouse CD8a	BV650	53-6.7	BioLegend	1:200
mouse CD11b	APC-Cy7	M1/70	BioLegend	1:100
mouse CD11b	APC	M1/70	BioLegend	1:100
mouse CD11b	FITC	M1/70	BioLegend	1:100

mouse CD39	PE-Cy7	Duha59	BioLegend	1:100
mouse CD39	APC	Duha59	BioLegend	1:100
mouse CD39	PE	24DMS1	Thermo Scientific	1:100
mouse CD45	BV786	30-F11	BioLegend	1:100
mouse CD45 for i.v. injection	perCP	30-F11	BioLegend	1:20 in PBS
mouse CD69	AF488	H1.2F3	BioLegend	1:100
mouse CD73	BV421	TY/11,8	BioLegend	1:100
mouse CD107a	AF700	1D4B	BioLegend	1:100
mouse CD186 (CXCR6)	PE/Dazzle594	SA051D1	BioLegend	1:100
mouse Ly6G	AF700	1A8	BioLegend	1:100
mouse P2X7	AF647	RH23A44	AG Nolte (UKE)	1:100
mouse SIINFEKL Dextramer	PE		Immudex	1:15
Sheep anti-mouse IgG	Dynabeads-M280		Invitrogen	1:40 (250 µl in 10 ml PBS)

Table 8: Enzymes

enzyme	**company**
polymerase	
Taq Dream DNA Polymerase	Thermo Scientific
restriction enzymes	
EcoRI-HF; 20,000 units/ml	NEB
NotI/NotI-HF; 20,000 units/ml	NEB
ligase	
T4 Ligase; 400,000 units/ml	NEB

Table 9: DNA-and protein standards

standard	company
GeneRuler, 1kb plus DNA Ladder	Thermo Scientific
PageRuler™ Prestained Protein Ladder, 10 to 180 kDa	Thermo Scientific

Table 10: Oligonucleotides (primers)

name	sequence
p07-forward	5'- GAGCTCACAACCCCTCACTC
p16-reverse	5'- GGCCTTATTCCAAGCGGCTT
p73-reverse	5'- GGGGCGGAATTTACGTAGC

Table 11: Plasmids and phagemids

gene of interest	vector
Entpd1 (Mouse CD39)	pCMV-Sport6
Nt5e (Mouse CD73)	pCMV-Sport6

Table 12: Pro- and eucaryotic cells

cells	company
prokaryotic cells	
XL-1 Blue competent cells	ATCC
eukaryotic cells	
bEnd.3	ATCC

Table 13: Mouse lines

mouse	official name
Brain Endothelial Ovalbumin (BrEndO)	C57BL/6-Tg(Slco1c1-icre/ERT2)1Mrks **x** Gt(ROSA)26Sortm2(OVA/EGFP)Dwir
OT-I	C57BL/6-Tg(TcraTcrb)1100Mjb/Crl

Table 14: Software

software	function
Endnote 20	reference manager
FlowJo 10™	data analysis flow cytometry
Light Cycler 96™ software	data analysis qPCR
GraphPad Prism 9	Data analysis, visualization, and statistical testing

2.2 Animal work and mouse lines

All animal experiments were approved by the local animal care committee (Behörde für Justiz und Verbraucherschutz der Freien Hansestadt Hamburg; Lebensmittelsicherheit und Veterinärwesen, Hamburg, Germany). The animal care proposals were registered under N19/087 and N22/018. All procedures were performed in accordance with the ARRIVE guidelines (Animal research: reporting of *in vivo* experiments).

The BrEndO mouse

The animal facility of the University Medical Center Hamburg-Eppendorf provided 8 to 14 weeks old BrEndO mice (Brain Endothelial Ovalbumin) derived from Slco1c1-CreERT2 mice crossed with RosaOVA mice (C57BL/6-Tg(Slco1c1-icre/ERT2)1Mrks x Gt(ROSA)26Sortm2(OVA/EGFP)Dwir). As depicted in Figure 1, the Slco1c1 promoter in front of the sequence coding for CreERT2 secures expression of CreERT2 in brain endothelial cells (Ridder et al., 2011). The Cre recombinase is fused to parts of the estrogen receptor (CreERT2). This CreERT2 fusion protein only enters the nucleus of a cell in the presence of tamoxifen, which is a drug binding to the estrogen receptor. In addition, RosaOVA mice carry an inverted cDNA sequence coding for ovalbumin, which is flanked by LoxP sites that are guiding the Cre-recombinase.

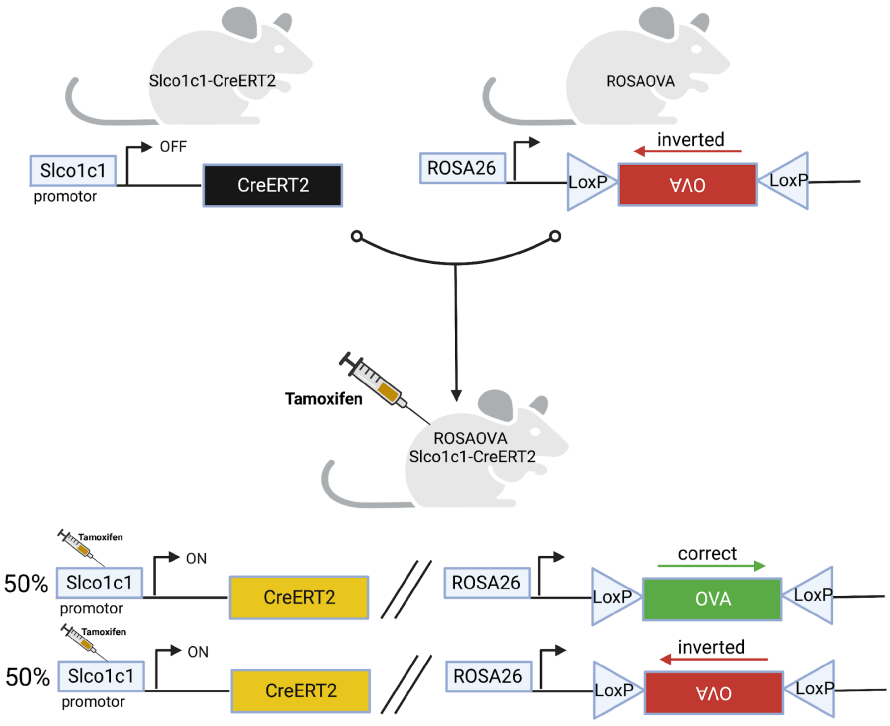

Figure 1: Genetic background of the experimental cerebral vasculitis mice. The Slco1c1-CreERT2 mouse carries a modified Cre recombinase fused to estrogen receptor parts (ERT2), that is expressed in cerebral endothelial cells due to the Slco1c1 promoter. The RosaOVA mouse holds an inverted ovalbumin coding sequence (OVA), which is flanked by LoxP sites. Administering 200 µl of Tamoxifen in corn oil (10mg/ml) prompts the Cre recombinase's entrance into the nuclei of cerebral endothelial cells. The inverted OVA sequence is flipped into the correct direction, resulting in ovalbumin expression and an OVA-specific CD8 T cell response at the BBB.

To induce experimental cerebral vasculitis, tamoxifen was dissolved in corn oil to a concentration of 10 mg/ml and 200 µl were injected intraperitoneally once a day for three consecutive days. Consequently, the Cre recombinase was expressed in cerebral endothelial cells flipping the inverted ovalbumin gene. When the ovalbumin gene flipps successfully, it is expressed and induces an anti-OVA CD8 T cell response against the OVA-expressing cerebral endothelial cells.

The OT-I mouse

OT-I mice express a T cell receptor specific for the OVA-derived SIINFEKL peptide presented in mouse MHC-I (Hogquist et al., 1994). OT-I CD8 T cells were used for adoptive transfer into BrEndO mice to analyze the impact of a CD8 T cell attack on brain endothelial cells. For this splenocytes of an OT-I mouse were

isolated on day 4 after injection of Tamoxifen into BrEndO mice (as described below). The prepared splenocytes were resuspended in 13 ml IMDM complete medium and seeded on a Greiner petri dish. The cells were stimulated with SIINFEKL peptide (stock 1 mM, 1:1000, 13 µl) for 18h in the incubator (37°C, 5% CO2).

On the next day (day 5), 250 µl of sheep anti-mouse IgG Dynabead was pipetted into a 15 ml falcon tube. The beads were resuspended in 10 ml PBS and placed in a magnetic stand for 5 minutes to magnetically attach to the wall of the falcon tube. PBS was discarded while the falcons were still standing in the magnetic stand. Meanwhile, the splenocytes were harvested from the petri dish and washed once with 10 ml PBS. The 10 ml cell suspension was transferred to the Dynabeads-containing falcon tube. The beads and cells were vortexed for 10 s. The falcon tube was then incubated on a gently shaking incubator (30 rpm for 30 min in a 4° C room) to deplete the B-cells bound to Dynabeads. After incubation for 30 min, the falcon was returned to the magnetic stand for 5 minutes. The supernatant was transferred to a fresh 15 ml falcon tube. The cells were washed twice with 10 ml PBS and centrifuged down (5 min 4°C). The B cell depleted cells containing mostly preactivated $CD8^+$ OT-I cells were resuspended in 10 ml PBS to dilute for cell counting in a Neubauer counting chamber. A cell suspension with a concentration of 3 million cells/ml PBS was then prepared for intravenous injection of 100 µl cell suspension i.v. containing 300,000 stimulated leukocytes.

2.3 Primary cell isolation from mouse organs

2.3.1 Anesthesia and mouse sacrifice

The mice were anaesthetized with low flow carbogen gas (CO_2/O_2) followed by exposure to pure CO_2. After ensuring that the mice had no further spontaneous respiratory attempts, the mouse neck was quickly dislocated. Finally, the neck dislocation was checked by placing the fingertip into the broken mouse neck.

2.3.2 Splenocyte isolation

The back of the sacrificed mouse was disinfected with 70% ethanol. The left side of the back was then cut open. The spleen was removed with two forceps and

placed in 5 ml cold PBS in a petri dish on ice. The spleen was then strained twice through a 70 µM cell strainer using the plunger of a 3 ml syringe. The PBS-splenocyte solution was then transferred to a 15 ml falcon tube, filled up to 14 ml with PBS, and centrifuged (310 g, 5 min, 4°C). 3 ml of erythrocyte lysis buffer was added to the cell pellet and the 15 ml falcon tube was vortexed. The cells were incubated for 3 minutes on ice. The reaction was then stopped by the addition of 3 ml PBS and centrifuged again (310 g, 5 min, 4°C). Finally, the supernatant was discarded and the splenocyte pellet was resuspended in 3 ml FACS buffer. By taking 200 µl of this suspension and transferring it through a 30 µm FACS tube filter into a FACS tube, approximately 1,5 million splenocytes were available for subsequent extracellular antibody staining.

2.3.3 Leukocyte isolation from brain parenchyma

The back of the sacrificed mouse was disinfected with 70% ethanol. The nose was fixed to the left and the tail to the right of a preparation board. A curved pair of scissors was then used to cut the neck and to open the skull through the foramen magnum. The skull was then opened right at eye level. The skull was removed with two forceps and the brain was removed with a spatula. The brain was placed in cold PBS in a small petri dish. The brain was then placed on the lid of the petri dish, sliced with a sharp knife, and transferred to 5 ml of a brain digestion solution in a 50 ml falcon tube and placed in a shaking water bath for at 37°C for 30 minutes. A 70 µm cell strainer was then placed on a new 50 ml falcon tube and the digested tissue was gently strained using the piston of a syringe. The previous tube was washed with 30 ml PBS and pipetted onto the 70 µm cell strainer. The 50 ml falcon tube was then centrifuged (310 g, 5 min, 4°C). The supernatant was discarded, and the cell pellet was resuspended in 5 ml Percoll gradient solution (33% Percoll and 66% 1x PBS). The Percoll-cell suspension was transferred to a new 15 ml falcon tube and centrifuged for 20 min without break function (310 g, 20 min, 4°C). The lymphocytes were now in the red cell pellet at the bottom of the tube. The supernatant was then discarded, and the walls of the tube were cleaned of myelin debris using a coiled paper towel. The erythrocytes were lysed with 3 ml erythrocyte lysis buffer for 3 minutes. The reaction was stopped by the addition of 10 ml FACS buffer and centrifugation

(310 g, 5 min, 4°C). Finally, the pellet was resuspended in 1 ml FACS buffer and transferred to a FACS tube for subsequent extracellular antibody staining.

2.3.4 Isolation of cerebral microvessels from mouse brain

This adapted protocol is based on a protocol published in Nature Methods (Lee et al., 2019). Prior to sacrificing the mice, chemicals had to be prepared. First, a 50 ml falcon containing 10 ml of 15% dextran-PBS was prepared per mouse by adding 1,5 g dextran to 10 ml PBS. The 50 ml falcons were shaken and vortexed. A 15 ml falcon with 5% BSA/PBS was then prepared by adding 0.5 g to 10 ml PBS. The MCDB 131 medium was then aliquoted into four 50 ml falcons (50 ml wash, 50 ml grinding, 50 ml petri dish and 50 ml extra) and cooled down in the refrigerator. A brain block was then placed on ice and forceps, scissors, a razor blade, a tissue grinder and a douncer were put on ice. Blotting paper (cellulose chromatography paper) was then prepared to remove the meninges during microvessel isolation. Finally, Petri dishes and 15 ml falcons were labelled with the mouse number and stored on a rack.

Immediately after brain preparation, the brain was placed in MCDB 131 medium in a Petri dish on ice. The brain was then rolled on the blotting paper to remove the meninges. The brain was placed inside an ice-cold brain block and cut sagittally into 4 slices of 2 mm diameter using a razor blade. The olfactory bulb and cerebellum were discarded. Importantly, the cortices were isolated using a fine metal spoon inside the dry lid of the Petri dish. The cortices looked like two crescents, which made it easier to separate them from the white matter, including the hippocampus. The cortical tissue was then homogenized using a tissue grinder. First, 10 initial strokes were made with a pestle in 1 ml of MCDB 131 medium inside the tissue grinder. The pestle was not rotated, and the speed of the strokes was medium. Then 1 ml of MCDB 131 medium was added to homogenize and two further strokes were made with the douncer. The homogenized tissue was then transferred to a 15 ml falcon tube. The tissue grinder itself was washed three time with 2 ml MCDB 131 medium and the contents transferred to the 15 ml falcon tube. The 15 ml falcon tubes were then centrifuged at 2000 g and 4°C for 5 mins. The supernatant was discarded, and

the 15 ml falcon tube was placed upside down on a paper towel to absorb excess medium and debris. The pellet was then resuspended in the prepared 1 ml of 15% dextran-PBS and pipetted up and down 5-6 times. Then 7 ml of dextran solution was added. The 15 ml falcon was centrifuged for 15 mins at maximum speed and 4°C (approx. 3500 g, recommended 10,0000 g). After this centrifugation step, a red microvessel pellet became visible. If that was not the case, the sample was contaminated with white matter substance, myelin, or other debris. After this maximum speed centrifugation, the supernatant was carefully removed with a serological pipette and later with a 1 ml pipette. Finally, the pellet was gently sluiced from this tube with 1 ml of PBS. The pellet was then transferred to a 40 µm cell strainer on top of a 50 ml falcon tube and washed with 9 ml of PBS. The microvessels were attached to the cell strainer, so the cell strainer was placed upside down on a new 50 ml falcon tube to retrieve them by adding 10 ml of 0.5% BSA/MCDB 131 in stages. The 50 ml falcons were then centrifuged again at approximately 3500 g (recommended 5000 g) and 4°C for 10 min. The supernatant was discarded, and the microvessel pellet was resuspended in the remaining small volume of supernatant and transferred as a solution to a 2 ml microcentrifuge tube. Then 200 µl MCDB131/BSA was added to the 2 ml microcentrifuge tube and the microcentrifuge tubes were centrifuged at maximum speed (10.000 g) and 4°C for 3 minutes. The supernatant was discarded by inverting the microcentrifuge tube. After that the RNA was isolated from the micro vessels.

2.4 Maintenance of bEnd.3 cells

To investigate brain endothelial cells in vitro we used the Balb/c derived bEnd.3 endothelioma cell line (Montesano et al., 1990).

bEnd.3 cells were grown in T75 cell culture flasks and fed with 10 ml DMEM Glutamax complete medium (10% FCS and 1% Penicillin/Streptomycin). Since this cell line is immortalized, the cells had to be split 1:3 once a week to avoid overgrowth. Prior to splitting, the old cell medium was removed, and the cells were washed with 10 ml prewarmed PBS. Then, the PBS was removed, and 3 ml preheated Trypsin-EDTA (0,05%) was added and distributed evenly (0,5 ml/10 cm^2). The bEnd.3 cells were incubated for 4 min at 37°C in the incubator.

Afterwards, the flasks were punched gently to ensure the loosening of the adherent cells. For a 1:3 split, 27 ml prewarmed DMEM Glutamax complete was added to 3 ml of Trypsin-EDTA. The FCS inside the medium was capable to inactivate the Trypsin-EDTA. Then 10 ml of the cell suspension were transferred to a new T75 cell culture flask. Every two days the old medium was removed and replaced by 10 ml prewarmed DMEM Glutamax complete.

To cryopreserve bEnd.3 cells, the cells were trypsinized as explained above, filled up to 14 ml with DMEM Glutamax complete and transferred into a 15 ml falcon tube. After centrifugation, the cell pellet was resuspended in 1 ml freezing medium containing 50% FCS, 40% DMEM and 10% DMSO and transferred into a cryotube. This cryotube was put inside a Propan-2-ol freezing chamber and placed inside the -80°C freezer.

For cell sorting, bEnd.3 cells were stained in 1 ml FACS buffer. The cells were sorted from a 1 ml cell suspension containing DMEM Glutamax complete into a 15 ml falcon tube lubricated with 1 ml pure FCS and 2 ml DMEM Glutamax. Finally, the sorted bEnd.3 cells were washed from sorting buffer using 10 ml DMEM Glutamax complete medium and transferred to a new T75 cell culture flask.

2.5 Production and cloning of lentiviral plasmids

For gene editing we used the CRISPR/Cas9 technique (Clustered Regularly Interspaced Short Palindromic Repeats) (Doudna and Charpentier, 2014).
We kindly received the LeGO-iG2/Neo-opt plasmid developed by Kristoffer Riecken (Center for Oncology, Interdisciplinary Clinic and Polyclinic for Stem Cell Transplantation, UKE) as a backbone to produce our own construct. This lentiviral backbone construct contains the sequence encoding for the Cas9 enzyme.
Together with preliminary work performed by former MD student Joschi Stabernack (Clinic and Polyclinic of Neurology, ERSI, UKE), we ordered guide DNA sequences after finding the best sequence using the CHOP-CHOP browser tool.

This procedure has been published before and was called SUCCESS method (Ishibashi et al., 2020). The authors showed that a cell line gene knockout can be achieved without constructing a new target vector with homologous for the 5` and 3` regions of every new gene (Ishibashi et al., 2020). This works by introducing two plasmids encoding Cas9 and guide RNA, two single-strand oligodeoxynucleotides and a universal selection marker sequence.
Finally, Kristoffer Riecken introduced these two plasmids into bEnd.3 cells with a stable lentiviral transfection. After three weeks in culture, transduced bEnd.3 cells did not release further virus particles and could be handled in a biosafety level 1 lab. Antibiotic resistance was used for selection of the stably transfected cells. The following explains the transformation and cloning procedure:

To incorporate the ordered plasmid DNA sequences into the lentiviral plasmid backbone, the restriction enzymes EcoRI-HF and NotI-HF were used. First, the lentiviral construct (LeGO-Ig2/Neo-opt) was digested in PCR tubes with 3 µl DNA, 2 µl CutSmart (10X by Roth), 1 µl EcoRI-HF (20,000 units/ml), 1 µl NotI-HF (20,000 units/ml) and 13 µl H_2O. Then, the PCR tubes were put into the cell incubator for digestion (37°C, 2h). An agarose gel was prepared by dissolving 1 g agarose in 100 ml TAE buffer inside a glass bottle (1%). The gel was dissolved in the microwave at 600 W for 3 min. Next, the dissolved gel was filled up to 100 ml with ddH_2O. Then 10 µl Roti gel stain (dilution 1:10.000 in 100 ml gel; concentration 20,000x by Roth) were added and the gel was transferred into a chamber and rested for 15 min. When the lentiviral construct and plasmid were completely digested, 3,4 µl of each were loaded into the gel. The first gel pocket was loaded with 10 µl DNA ladder 1 kb. The gel was started at 120 V and ran for 45 min. After that, a transilluminator machine was used for DNA band identification.
Last, the gel bands were purified in a 2 ml microcentrifuge tube according to the MN-Kit purification protocol. The constructs DNA concentration was measured using the Nanodrop analyzer.
After successful digestion of the new plasmid and the lentiviral construct backbone, the ligation was continued. The ligation was done using 50 ng lentiviral construct DNA, 5 µl insert DNA, 10 µl 2x Quick ligation buffer, 1 µl Quick Ligase

and filled up with ddH_20 to 20 µl (concentration ratio lentiviral construct 1:10 insert DNA). The ligated product was incubated at room temperature for 10 min. Finally, it was chilled on ice and sent for sequencing to Eurofins using 1500 ng of plasmid DNA diluted with H_2O to 17 µl total volume. Then either 2 µl of a forward or a backward primer (10 pmol/µl) were added. The sequencing result was downloaded from the Eurofins webpage and aligned to the original plasmid sequence using the alignment function of the Nucleotide BLAST tool by the U.S. National Library of Medicine.

Next, the successfully generated lentiviral plasmids were transferred into XL1 E. coli bacteria. First, the bacteria were taken from the -80°C freezer and thawed on ice. Then, 50 µl bacteria solution was transferred to a 15 ml falcon tube. Around 1 ng DNA plasmid was added to the bacteria and incubated on ice for 30 minutes. In the meantime, SOC-medium was preheated to 42°C. Then, the solid LB-Agar was liquified in a microwave. The LB-Agar was cooled down until the temperature was around 60°C. Moreover, a carbenicillin aliquot (20 mg/ml) was thawed up and 10 µl of antibiotic were added to 10 ml LB-Agar (1:1000, 20 µg/ml) and poured into a Petri dish. Then, the bacteria were heat shocked for 45s in the 42°C water bath and put on ice immediately for 2 min. 450 µl of warm SOC medium was then added to the bacteria. During the next hour the bacteria were gently shaken (30 rpm, 4°C 1h). Afterwards 150 µl of bacteria and sterilized small glass balls were added to the prepared LB-agar plate. The LB-agar plate was shaken gently to distribute the bacteria on the plate and then put inside a bacteria incubator upside down overnight for up to 16 h at 37°C.
In the morning of day 2, the LB-Agar plates were checked for bacteria colonies. One of the colonies was picked using a 10 µl pipet tip and thrown into either an Erlenmeyer flask containing 100 ml LB medium (Maxi Prep) or into a 15 ml falcon tube containing 5 ml of LB-medium both with 1:1000 carbenicillin antibiotic. The LB-medium vials with the picked colonies were incubated inside a shaking bacteria incubator at 37°C for up to 16 h.
On day 3 or after 16h of incubation, the Erlenmeyer flask or the 15 ml falcon tube were checked for bacteria expansion. The volume of the Erlenmeyer flask was transferred to two 50 ml falcon tubes and centrifuged down for 30 min at

maximum speed of the centrifuge. Then the plasmids were purified using the provided Qiagen Mini Prep or Maxi Prep protocol. Importantly, after finally eluting the plasmid from a DNA column, the column was rested for 5 min and then centrifuged for 1 min again. This increased the concentrations of DNA. The eluate concentrations and A260/280 DNA to protein light emission quotient for purity were then measured at a Nano Drop machine. A Qiagen Maxi-Prep yielded 500 µg of plasmid after cloning, whereas 30-50 µg of plasmid could be yielded after Qiagen Mini-Prep.

Moreover, after amplifying the DNA plasmid, the new candidates were sent for sequencing to Eurofins again and their sequence aligned to the desired plasmid sequence using the Nucleotide BLAST tool.

2.6 Cell culture assays and RNA isolation

2.6.1 AMP Glo assay to measure CD73 activity

The AMP Glo assay is a luciferase-based assay to quantify extracellular AMP. First, ATP is consumed to convert luciferin to luciferin adenylate by binding of AMP to luciferin. Second, the luciferase catalyzes the excitation of luciferin adenylate. Third, the luciferin adenylate falls back to ground state and reacts to form oxyluciferin by splitting off CO_2. The energy released in the third step is emitted as light as shown in Figure 2.

Figure 2: AMP Glo assay principle (scheme adapted by Promega). A luciferase-based method quantifying extracellular AMP. The AMP Glo kit comprises two reagents: the first halts AMP generation, removes ATP, and converts AMP to ADP. The second reagent transforms ADP back to ATP, fueling the luciferase reaction's luminescence.

The performance of this assay has been adapted from a published protocol to monitor CD73 enzyme activity (Goueli and Hsiao, 2019). First, trypsinized bEnd.3 cells were diluted to 250.000 cells/ml. Then 100 µl form this dilution (25.000 cells) are transferred as triplicates to a 96 well plate for cell culture. Next, 100 µl DMEM

containing 20 µM AMP were added (stock 10 mM, 1:500 dilution) to reach a final concentration of 10 µM in a total volume of 200 µl. Then, the AMP was incubated with the cells on ice for 40 minutes. In the meantime, the AMP-Glo Reagent I was brought to room temperature and AMP detection solution (reagent II) was thawed up on ice for at least 30 minutes. After 40 minutes of AMP-cell incubation, the 96 well plate was centrifuged (310 g, 5 min, RT). 25 µl of the supernatant from each triplicate was transferred to a white bottom 96 well plate suitable for a luminometer (e.g., Victor Reader). Then 25 µl AMP-Glo Reagent I (RT) were added and resuspended and incubated for 30 minutes at RT. In the meantime, the AMP-Glo detection solution was prepared by mixing 1 ml Kinase-Glo one solution with 10 µl AMP-Glo Reagent II. 50 µl of this AMP-Glo detection solution were added to the supernatant in the white bottom 96 well plate and incubated for 60 min at RT. Finally, the plate was read using a luminometer (e.g., Victor Reader) and the results were exported to Excel. These results were then transferred to Prism 9 and displayed as bar graphs to compare different CD73 enzyme activity of modified bEnd.3 cells.

2.6.2 RNA isolation from cells

The Qiagen RNA Preparation Mini Kit was utilized for RNA isolation. Initially, the target cell type was centrifuged at 350 g and 4°C for 5 minutes, followed by resuspension of the cell pellets in 350 µl RLT lysis buffer. Vortexing for 10 seconds ensued. Cells adhering, such as cerebral endothelial cells, were lysed directly in a well plate. The resulting lysate was then transferred to a gDNA binding column and centrifuged at 8000 g and 18°C for 30 seconds. Subsequently, the flow-through was mixed with 350 µl of 70% ethanol and moved to an RNA binding column. Centrifugation followed at 8000 g and 18°C for 30 seconds, and the flow-through was discarded. The RNA binding column underwent a wash with 700 µl RW1 buffer at 8000 g and 18°C for 30 seconds, with the flow-through being discarded again. A second washing step employing 500 µl RPE buffer was performed at 8000 g and 18°C for 30 seconds, repeated with an extended centrifugation time of 2 minutes. The RNA binding columns were placed in new 2 ml microcentrifuge tubes and dried with an open lid at 21,000 g and 18°C for 1 minute. Finally, these columns were transferred to new

1.5 ml microcentrifuge tubes, and 30 µl of RNase-free water was added to the membrane. A final centrifugation at 8000 g and 18°C for 1 minute facilitated the elution of the bound RNA from the column, which was subsequently stored at -80°C.

2.7 Gene expression analysis

2.7.1 Production of complementary DNA and quantitative PCR

The reverse transcriptase facilitates the creation of single-stranded complementary DNA (cDNA). The Maxima synthesis kit compounds were employed for this cDNA synthesis process. Initially, RNA isolation was quantified using a NanoDrop device. To ensure adequate cDNA synthesis, a minimum RNA concentration of 20 ng/µl and a 260/280 ratio of approximately 2.0 (RNA/protein light emission) were targeted. Once measured, the RNA samples were stored on ice.

For the cDNA synthesis, new 500 µl microcentrifuge tubes were labeled, indicating Cre status, mouse number, date, type of nucleic acid, and the date of processing. Subsequently, 7 µl of nuclease-free water was added to each labeled microcentrifuge tube. A master mix of 6 µl per sample was then prepared in a separate microcentrifuge tube per RNA sample, consisting of 4 µl nucleotide reaction mix (5x) and 2 µl of reverse transcriptase. This master mix (6 µl) was added to the 7 µl of nuclease-free water. Finally, 7 µl of RNA was pipetted into each microcentrifuge tube (1:2 dilution) to achieve a final volume of 20 µl.

The microcentrifuge tubes containing the samples were transferred to a PCR cycler device (Eppendorf, Master cycler gradient) to undergo the cDNA synthesis program. Initially, the samples were incubated at 25°C for 10 minutes. Subsequently, the temperature was raised to 50°C and maintained for an additional 30 minutes. Finally, the samples were heated to 85°C for 5 minutes to halt the reverse transcriptase activity.

The synthesized cDNA was then diluted at a ratio of 1:25 with RNAse-free water, combining 10 µl of cDNA with 240 µl of RNAse-free water. If desired, the cDNA could be stored at -20°C for future use.

In principle, this cDNA material is used for quantitative polymerase chain reaction (qPCR), which is based on fluorochrome coupled primers (taqman probes).
In essence, this cDNA material is utilized in quantitative polymerase chain reaction (qPCR), a process reliant on fluorochrome-coupled primers (TaqMan probes). Typically, these probes' fluorochrome activity is subdued by a Quencher. As the strand fills up in a PCR cycle, the DNA polymerase severs the Quencher. Consequently, a fluorescence signal is emitted in proportion to the cDNA material bound to the TaqMan probe. The analysis involves calculating the cycle exhibiting exponential fluorescence signal amplification. The normalization of target gene PCR cycles is achieved with a stably expressed housekeeping gene (HKG).
First, a master mix with 5 µl “Maxima probe qPCR master solution” and 0,5 µl target taqman probe P2rx7 (Mm0040582_m1) and CD73 (Mm00501910_m1) were prepared in a 500 µl microcentrifuge tube. As a housekeeping gene, Sdha (Mm01352366_m1) was used. This gen is responsible for the mitochondrial respiratory chain and has a stable expression. Each time, 5,5 µl of the master mix were added to a special qPCR 96 well plate and 4,5 µl cDNA (1:25 diluted) was added. Importantly, each well was resuspended with a fresh pipet tip. For each cDNA sample, triplicates for housekeeping gene and target gene were prepared. After that, the qPCR well plate was centrifuged (350 g, 4°C, 5 min). Finally, the plate was placed in the LightCycler96, and the qPCR program was run.
The results of the measurement were sent per email automatically. The LightCycler96 software was used to find outlier Cq values and exclude them from Cq mean calculation. Then, the mouse numbers, Cq and Cq mean values were copied to Excel. An Excel analysis template sheet was created. First, the Cqt mean(target) values were subtracted by the corresponding Cqh mean (housekeeping gene) values. Next, the mean of these dCt values for biological replicates was calculated. Afterwards, the dCt values were normalized to the control condition (f.e. unstimulated samples) by subtracting the normalized dCt from the sample dCt values. Further, the fold change of these normalized values was calculated by potentiating the negative normalized dCt values with the basis 2 (POTENZ(2;-dCt normalized). Finally, the mean of the fold change was calculated as well as the standard deviation of the fold change values for all

biological replicates. These values were transferred to Graph Pad Prism in a grouped table and checked for significant expression fold changes using a Student's t-test.

2.7.2 RNA sequencing

The process of next-generation sequencing involves four main steps: Fragmentation, adaptation, amplification, and data analysis. During sample preparation, the genomic DNA is fragmented, and sequencing adapters and unique barcodes are attached to the ends of the fragments. The barcodes help in identifying and analyzing multiple samples simultaneously, while the sequencing adapters enable binding of the DNA fragments to the flowcell, which is a glass slide containing immobilized oligonucleotides for amplification and sequencing.

After combining the sample fragments with sequencing adapter barcode complexes into a library, they are loaded onto the flowcell, where the DNA fragments bind to the immobilized oligonucleotides and undergo bridge amplification, resulting in clonal clusters with identical DNA fragments. The sequencing process then begins using the Sequencing By Synthesis (SBS) method, where a mix of labeled dNTPs bind to the DNA fragments in a complementary manner, followed by detection in the spectrum of green and red wavelengths.

Once the sequencing is complete, the detected sequences are evaluated using bioinformatics by aligning them against the reference genome and combining them into a consensus sequence to identify any changes. These changes are then assessed for clinical relevance, and the results are presented in a report. The 2-channel SBS technology used in NextSeq sequencing allows for significant time and cost savings by using two colors to detect four nucleotides (Qin, 2019).

2.7.3 Flow cytometry

In flow cytometry a suspended single cell sample is streaming through a laser beam. The lasers can excite certain cell components and fluorescently labeled cells, which leads to light emission in a certain wavelength range. This optical signal is processed by photodetectors coupled to photomultipliers converting

these signals into electronic pulses. These electronic pulses can be visualized and interpreted by software (“Flow Cytometry - Orbit Biotech”). Thus, flow cytometry allows a multiparametric analysis of the physical properties of cells such as cell size, granularity as well as detection of cell antigens or markers present either on the surface or cytoplasm and nucleus. The intensity of the fluorescent protein coupled antibody emission is proportional to the number of the targeted antigens and the natural brightness of the used fluorochrome. Moreover, the fluorescent emission of some fluorochromes overlaps on the wavelength spectrum. Thus, the spill-over of one fluorochrome emission into another detector channel must be subtracted from the detected emission signals in the other detector channel. This can be achieved by measuring single-stained wild type spleen cells or compensation beads loaded with the respective fluorochrome-labeled antibody.

Trucount tubes

A BD Trucount tube contains a lyophilized exact number of beads with the same size that can be detected with a flow cytometer using a forward scatter (FSC) vs. side scatter (SSC) dot plot (Figure 3). Since the beads are phycoerythrin (PE) conjugated, the PE channel can be used to verify the selected events from FSC-A/SSC-A gating.

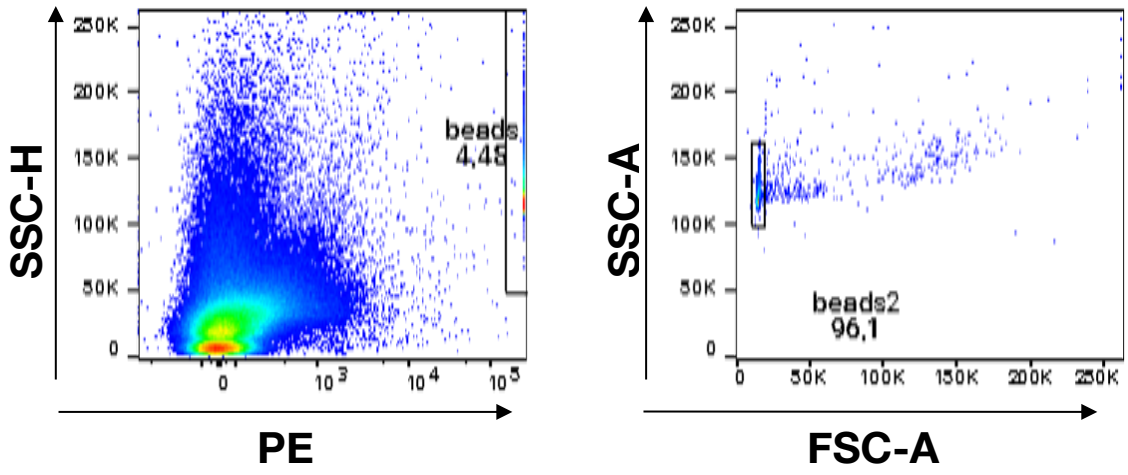

Figure 3: Gating strategy for BD Trucount tubes for the calculation of absolute cell numbers. First, the Trucount beads are identified by gating for a high phycoerythrin conjugated population. Second, the selected events are verified by gating for a homogenous small population in the FSC-A/SSC-A plot.

Cell surface antibody staining

A master mix containing all antibodies in the appropriate dilution (see material table) was prepared containing 100 µl FACS buffer including the diluted antibodies was prepared for one FACS tube with an immune cell pellet. Beforehand, the FACS antibodies were vortexed and added to a black microcentrifuge tube which was protecting the fluorochromes from light. The cells were incubated in 100 µl master mix per FACS tube for 30 min at 4°C in the dark fridge. Afterwards, the cells were washed with 2 ml FACS buffer and centrifuged for at 310 g and 4°C for 5 minutes. Finally, they were resuspended in 200 µl FACS buffer for flow cytometer analysis.

Legendplex cytokine beads for flow cytometry

“The LEGENDplex TM mouse Th Cytokine Panel was used as a bead-based multiplex assay panel, using fluorescence–encoded beads suitable for use on various flow cytometers. This panel allowed simultaneous quantification of 12 mouse cytokines, including IL-2, 4, 5, 6, 9, 10, 13, 17A, 17F, 22, IFN-γ and TNF-α. First, all reagents had to be brought to room temperature. The 20x wash buffer was diluted 1:20 by taking 25 ml and adding 475 ml deionized water. Second, the lyophilized Mouse Th Panel Standard cocktail was dissolved in 250 µl Assay Buffer according to its lot number. The standard cocktail was left at room temperature for 10 minutes. Six new 1,5 ml microcentrifuge tubes were labeled C6 – C0 and 75 µl assay buffer were added to each of the six tubes. Then, the top standard (C7) was diluted 1:4 to an appropriately labeled polypropylene microcentrifuge tube (C6) by transferring 25 µl from C7 to C6. This was continued until C1. C0 was prepared as the blank control containing only Assay buffer.

Afterwards, the delivered V bottom plate was prepared with duplicates for the standards and the cell culture supernatant samples. First, 25 µl Assay buffer were added to each well duplicate. Then, 25 µl standard or 25 µl sample were added to each well duplicate. Third, the mixed beads were vortexed for 30s. Then 25 µl of mixed beads were added to each well to a total volume of 75 µl. The V bottom plate was then sealed with a plate sealer and covered in aluminum foil. It was shaken at 600 rpm on a plate shaker at room temperature for 2 hours. After that, the plate was centrifuged at 250 g for 5 min. Immediately after centrifugation, the

blue beads could be seen at the bottom of the well and the supernatant was dumped into a sink by quickly inverting the plate and letting dry on a paper towel. Then, 200 µl 1x Wash Buffer were added using a multipipet for 1 min. The plate was centrifuged again as above, and the supernatant was discarded into the sink again. After that, 25 µl of detection antibodies to each well. The plate was once again sealed with a new plate sealer. The entire plate was covered in aluminum foil again and shaken at 600 rpm on the plate shaker at room temperature for 1 hour. Importantly after 1 hour the plate was not washed, but 25 µl of Streptavidin-PE antibodies were added to each well directly. Then the plate was sealed again using a new plate sealer and covered with aluminum foil. It was shaken again at 600 rpm at room temperature for 30 min. Afterwards, the plate was washed by dispensing 200 µl of 1x wash buffer into each well and letting incubate for one minute. Centrifugation and dumping of the supernatant were repeated as explained above. Then 150 µl 1x wash buffer was added to each well and the beads were resuspended by pipetting. The plate was ready to be read on a flow cytometer using FACS tubes. Importantly, the FSC and SSC were used to distinguish Beads A and Beads B. Next, the APC and PE channel voltage were set to detect 6 different beads intensities each corresponding with the 12 cytokines that could be detected. In total, around 10.000 events were recorded for sufficient analysis. The FCS files were analyzed using the web browser based LEGENDplex Data Analysis software.

2.8 Recombinant production of P2X7-blocking nanobodies

2.8.1 Production and purification of bivalent P2X7 nanobodies

The plasmid of the inhibiting 13A7 nanobody was used to transiently transfect HEK-6E cells (A). After six days, the recombinant nanobodies were purified from the cell supernatant by Nickel-NTA purification columns (B) and 10 µl of the supernatant were analyzed on an SDS-PAGE gel using Coomassie brilliant blue staining (C) (see Figure 4).

(A) Transfection of HEK-6E cells

On day 0, the HEK-6E cells were split 1:5 by taking 6 ml from 30 ml total medium volume inside a T175 green suspension cell culture flask. These 6 ml were

transferred to a new T175 flask already containing 24 ml pre-warmed F293 cultivation medium. On day 1, 7,5 mM polyethylimine, 300 mM NaCl ,and sterile H2O was pre-warmed in the water bath at 37°C for 30 minutes. In the meantime, the plasmid DNA was thawed up at room temperature. Per T175 flask 1 ml of PEI Mix and 1 ml the plasmid DNA mix were prepared inside to separate 15 ml falcon tubes. For the PEI mix, 248 µl 7,5 mM PEI (160 µg) were filled up to 500 µl with H2O and 500 µl 300 mM NaCl were added. For the DNA mix, 20 µg of DNA were filled up with H_2O to 500 µl and 500 µl 300 mM NaCl were added. Importantly, the PEI mix was vortexed and added slowly dropping to the 500 µl DNA mix. Then, the DNA-PEI-mix was vortexed for 10 seconds and incubated for 30 minutes at room temperature. Then the 2 ml DNA-PEI-mix were added dropwise to the T175 flask containing 30 ml HEK-6E cell suspension. On day 2, 750 µl of feeding medium were added to the T175 flask containing F293 medium + 20% tryptone. On day 6, the supernatant was harvested by transferring to the medium and HEK-6E cells to a 50 ml falcon tube and centrifuging at 310 g and 4°C for 5 min. The supernatant was then filtrated using a vacuum protein filtration tube.

(B) Nickel-NTA nanobody purification

The nanobodies were purified by the binding of Nickel reagents to their histidine rests. The working bench was prepared with a metal kickstand to hold the purification columns and 50 ml falcon tubes in a rack to save the flow through from each step of purification. Per purification column, 10 ml binding buffer and 20 ml washing buffer were prepared by diluting the 4x stocks 1:4 with deionized water. Then, the Ni-NTA Agarose buffer was taken from the fridge and inverted many times until the solution became soluble. Per column 4 ml of Ni-NTA Agarose were added into the column. When the Ni-NTA Agarose buffer reached the 2 ml mark of the purification column, then a new filter was pushed until the 2 ml mark of the column using the back of a 10 ml serological pipet. After that, 10 ml binding buffer were added to the column. Then the 30 ml supernatant from one T175 cell culture flask was added to the column. The flow through was collected in a 50 ml falcon tube. Then the column was washed with 20 ml 1x washing buffer and the flow-through was stored in a new 50 ml falcon tube. Finally, HIS Select Elution buffer was used to collect the eluates from the column

in 4x 2 ml microcentrifuge tube using 1 ml elution buffer for the first 2 ml microcentrifuge tube and 2 ml elution buffer for the second, third, and fourth microcentrifuge tube.

After that, an AMICON tube with the correct membrane pore size was chosen to increase the concentration of the target nanobody. Since the nanobody size was around 50 kDa, an AMICON tube with 30 kDa membrane was chosen to keep only proteins with a size bigger than 30 kDa. A maximum of 10 ml could be added to the column and 3 times more PBS with Mg^{2+} and Cl^- were added step by step to the eluate volume to wash out the eluate buffer. This step was performed sterile under the cell culture hood. After several centrifugation steps at 4000 g and 4°C for around 10 minutes each time, the protein was recovered in 1 ml clear PBS by pipetting up and down on the AMICON tube membrane. A 10 µl aliquot was stored in a small PCR tube for analysis on an SDS-PAGE gel. The 1 ml nanobody in PBS containing magnesium and chloride was transferred to a cryotube and immediately brought to the -80°C freezer.

(C) SDS-PAGE gel to verify successful nanobody purification

First, the nanobody was denaturized in small transparent PCR tubes in a 10 µl solution containing 6,5 µl sample, 2,5 µl LDS sample buffer (NuPAGE LDS buffer, lithiumdodecylsulfate, 4x) and 1 µl reducing agent (NuPAGE, 10x, 50 mM Dithiothreitol DTT) from the fridge. A mix of LDS sample buffer and reducing agent was prepared in a 500 µl microcentrifuge tube. These samples were then heated in a heat block at 70°C for 10 minutes to denaturize the proteins. In the meantime, 1x NuPAGE MES was prepared by diluting 25 ml 20x NuPAGE with 475 ml deionized water. The Electrophoresis Mini-Cell chamber by Invitrogen was filled with 500 ml 1x NuPAGE. Then the NuPAGE 4-12% Bis-Tris Gel with 15 gel wells was placed inside the Mini-Cell chamber. A Prestained protein ladder 10-130 kDa (PageRuler) was loaded to the first well of the SDS PAGE gel. Then, the denaturized flow through, washing buffer flow through, eluate 1-4, the AMICON tube and the AMICON tube flow through were loaded into the wells. These 8 samples in total plus the 1 kb ruler were used to visualize any loss of nanobody in the process of purification. The gel was run at 185 V for 40 min. After that, the gel was detached from the hard plastic cover and put into a plastic box with VE-

water on the shaker for 3 times 5 minutes. Afterwards, the gel was covered with Bio-Coomassie and gently shaken for 1 hour inside the plastic box. Then, the Bio-Coomassie stain was dispensed, and water was added to the SDS-PAGE. After a few hours on the shaker, gel bands became visible. Finally, this gel was scanned on a regular scanner with 300 dpi.

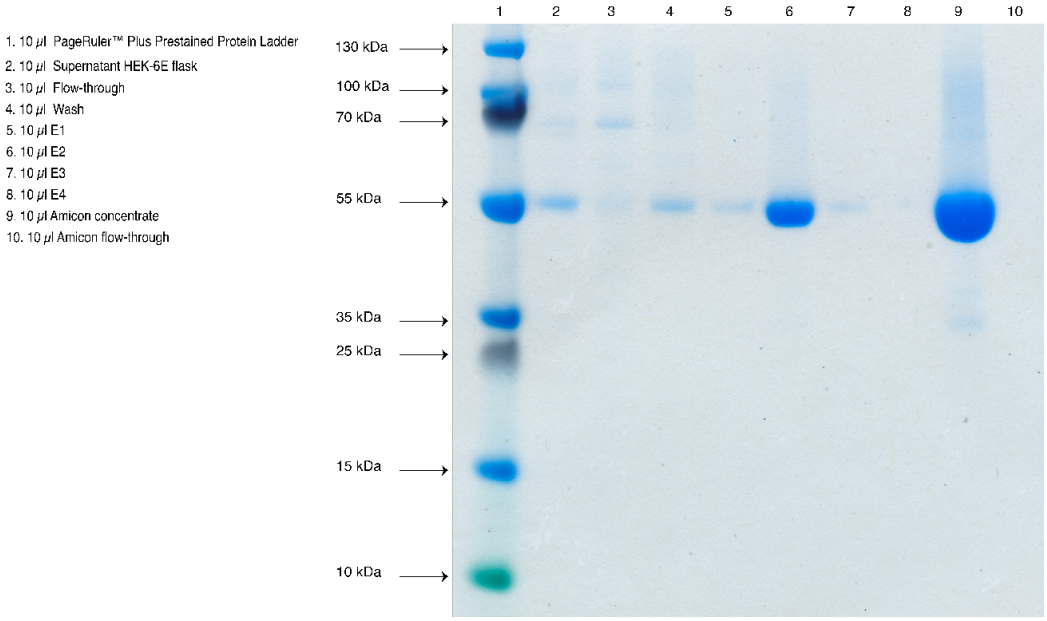

Figure 4: SDS-PAGE gel showing the purification of the inhibiting P2X7 nanobody (13A7 dim-Alb). The wells were loaded with 10 µl aliquots of denaturized protein samples: Lane 1: Ladder, Lane 2: HEK-6E supernatant 13A7 nanobody, Lane 3: unbound protein fraction (flow-through), lane 4: column washing, lane 5-8: eluates 1-4 (2ml each), lane 9: Amicon tube protein concentrate, lane 10: Amicon tube flow-through.

2.8.2 Measuring the concentration of P2X7 nanobodies

The concentration of the nanobodies was measured by Bicinchoninic acid assay (BCA). A standard curve of bovine serum albumin concentrations (0.125, 0.5, 0.75, 1.0 mg/ml) was used to calculate a tangent equation in Excel (see Figure 5). This equation could be solved by X to calculate the concentrations of the control nanobody, 13A7 and 14D5 nanobodies. After solving the tangent equation for X, the concentrations had to multiplied by 10 according to the manufacturer protocol. Thus, the concentrations of the nanobodies were 1.8 mg/ml (control), 6.5 mg/ml (13A7), 8.2 mg/ml (14D5).

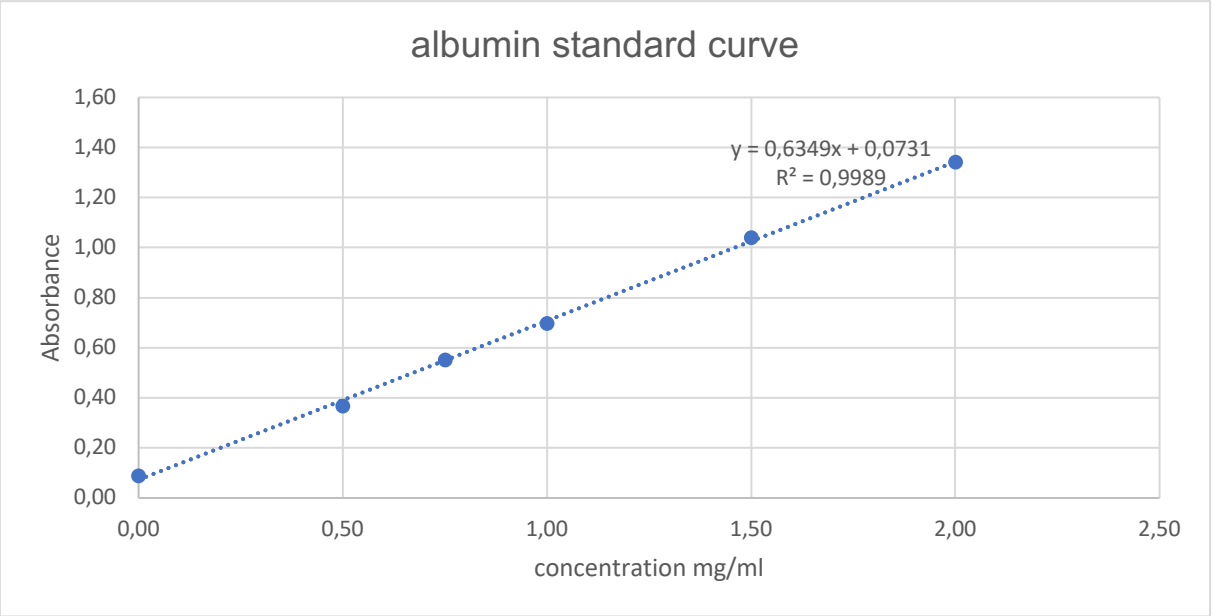

Figure 5: Albumin standard concentration titration results in a tangent equation. By solving this equation for X, the corresponding concentration for each nanobody can be calculated

BCA for protein quantification

To measure the concentration of the nanobodies, the Piere BCA Protein Assay kit by Thermo Scientific was used. The principle was the reduction of Cu2+ to Cu+, which was able to build a color complex with BCA. This complex was analyzed colorimetric using an ELISA reader at 560 nm. Fist, reagent A and reagent B were mixed 1:50. 190 µl of the reagent mix were prepared per well of a 96 well ELISA plate. Then, a BSA (albumin) titration was added to the wells in duplicates to get 0, 0,25, 0,5, 0,75, 1, 1,5 and 2 mg/ml for the standard curve. The nanobody eluate samples were diluted using 2 µl sample and 8 µl of deionized water. Then, the ELISA plate was incubated at 37°C for 30 min. Finally, the ELISA plate was read using an ELISA reader and the BSA computer program. The luminescence values from the ELISA reader were analyzed in Excel by calculating the standard means and doing a linear regression graph with a tangent equation. By solving the tangent formula for x, the concentrations of the samples could be calculated.

3. Results

The results are presented in three chapters. Chapter 3.1 introduces the experimental brain endothelial ovalbumin (BrEndO) mouse model and characterizes the immune cells that drive the inflammatory disease. Chapter 3.2 focuses on the pro-inflammatory ATP receptor P2X7, which can be inhibited by a nanobody (clone 13A7). In addition, I characterized the expression of purinergic molecules on microvessels isolated from the BrEndO mouse brain. Finally, section 3.3 presents a pipeline to generate a genetically modified endothelial cell line *in vitro*. Here, the expression of three purinergic enzymes in a cerebral endothelial cell line were altered using a lentiviral transduction system.

3.1 Characterization of immune cells in the BrEndO mouse model

3.1.1 BrEndO mice elicit an endogenous anti-SIINFEKL CD8 T cell response

The BrEndO mouse was developed as a Tamoxifen inducible model to mimic immunological features as they might occur in patients with primary cerebral vasculitis. Figure 6A shows the experimental design with a daily Tamoxifen injection for three consecutive days. The peak of the disease was marked by weight loss around day 11. Immune cells were isolated from the brain of BrEndO mice at d11 and d25 at the end of the experiment. The isolated immune cells were subsequently stained with fluorochrome conjugated antibodies to identify different immune cell subpopulations using a flow cytometer.

It was observed that the body weight of the mice develops differently from day 8 to day 25 (Figure 6B). Whereas Cre+ BrEndO mice weight approximately 104% of their initial weight at day 11, Cre- mice control mice weight around 112% of their initial weight. Some of the Cre+ BrEndO mice even dropped below their starting weight. Subjectively, this finding correlated with the appearance of neurological symptoms in these particular mice, as the animals had a more tense posture and became less active around day 11. The Cre+ BrEndO mice did not reach the weight of the control group at the end of the experiment (d25). However, Cre+ BrEndO mice were devoid of visible symptoms at day 25.

Figure 6C displays the general gating strategy for the immune cells isolated from the BrEndO mouse brain on day 11. First, we gated for all CD45 positive immune cells. Then we gated for CD11b negative leukocytes to exclude granulocytes, monocytes, and microglia. Next, we gated specifically for CD3 T cells to finally distinguish between CD4 T cells and CD8 T cells. When comparing the gating for immune cells in a Cre- control mouse in the upper row to the gating in a Cre+ BrEndO mouse in the lower row, we identified a profound increase in leukocyte infiltration into the brain in general. Specifically, we see more T cell infiltration,

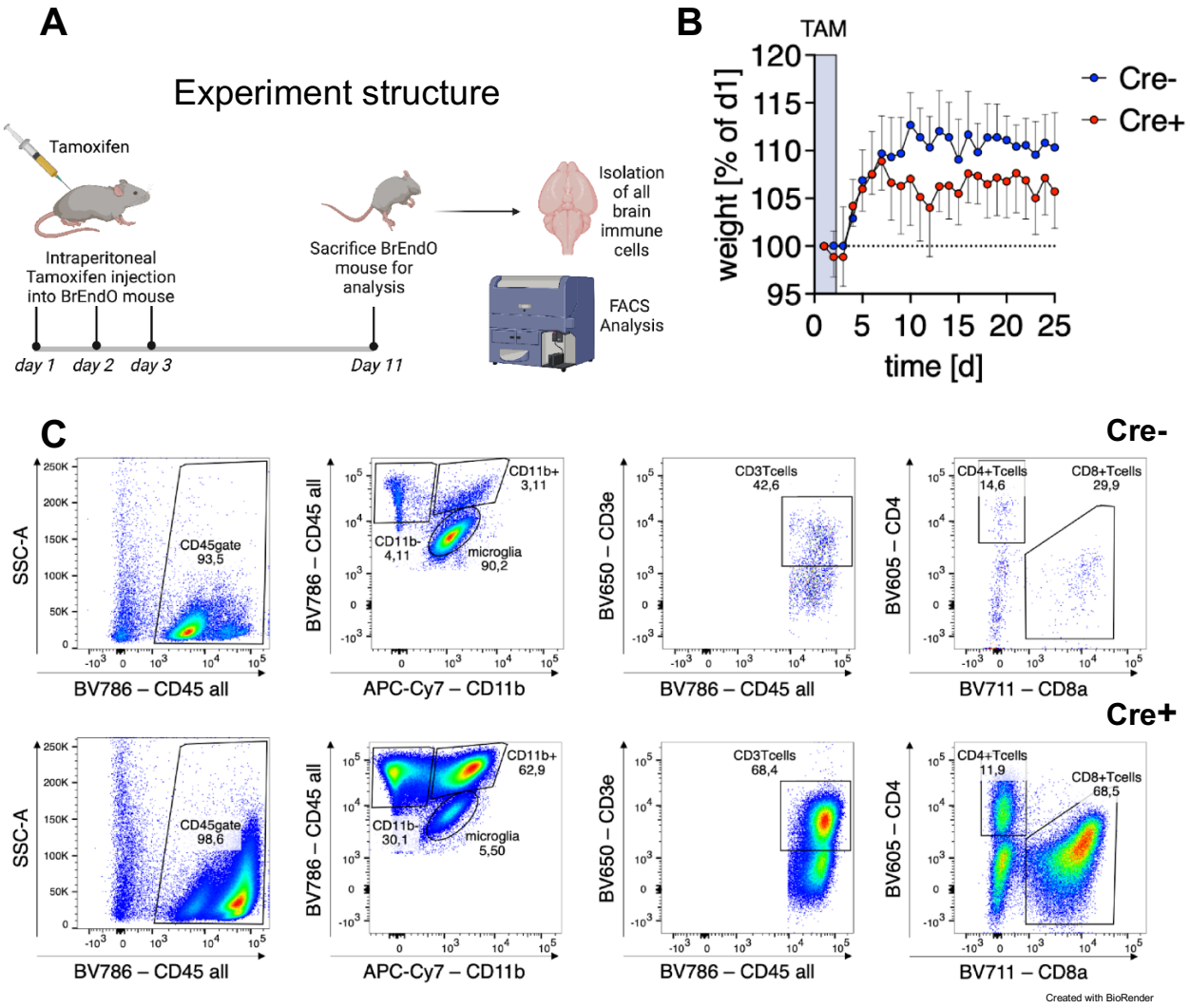

Figure 6: Flow cytometric analyses of brain infiltrating immune cells in the BrEndO mouse model.
(A) Experiment setup with OVA induction via Tamoxifen injections and immune cell isolation from the brain on day 11. (B) The weight of Cre+ (red) BrEndO mice and Cre- (blue) control mice was normalized to day 1 and monitored throughout the experiment. (C) Flow cytometry gating strategy to identify immune cells from the brain comparing Cre- control and Cre+ BrEndO mice. TAM = Tamoxifen

which was dominated by CD8 T cells. Thus, we focused on the investigation of CD8 T cell subpopulations that infiltrate the BrEndO mouse brain.

3.1.2 Distinguishing vascular and parenchymal leukocytes: A flow cytometry approach using intravascular CD45 labeling and a SIINFEKL-Dextramer

Neuroinflammatory diseases are characterized by the compromised integrity of the blood-brain-barrier (BBB) and subsequent immune cell infiltration into the brain parenchyma. To distinguish vascular leukocytes from intra-parenchymal leukocytes, fluorochrome-labeled antibodies against the pan-leukocyte marker CD45 can be injected intravenously shortly before sacrificing the mouse. This approach labels all vessel-resident immune cells, whereas cells residing in the parenchyma are not labeled. For this, BrEndO mice were injected with perCP-conjugated anti-CD45 i.v. into the tail vein and sacrificed 3 min after injection (Figure 7A). Afterwards, we took out the brain for immune cell isolation. Additionally, to the cell surface antibody staining, we used a so called “dextramer” made of 6 MHC-I molecules loaded with the ovalbumin-derived peptide SIINFEKL. This allows the identification of SIINFEKL-specific CD8 T cells within the CD8 T cell population and together with the injected perCP-conjugated anti-CD45 antibody reveals whether the cell is in the vasculature or the parenchyma. Figure 7B and 7C show an exemplary flow cytometry dot plot and a pie chart with the mean percentages for the subpopulation quadrants of CD4 and CD8 T cells. Given the mean percentages in the pie chart in Figure 7C, approximately 32% of the CD8 T cells are SIINFEKL-specific (Dex+) and are located inside the brain parenchyma (IV-). Around 55% of the CD8 T cells infiltrated the brain parenchyma (IV-) and are not specific for SIINFEKL. The CD8 T cells in the vasculature appear evenly distributed with around 6% SIINFEKL-specific and unspecific subpopulations. Regarding Figure 7C, around 90% of the CD4 T cells reside inside the brain parenchyma (IV-) and are, as expected, not specific for the SIINFEKL peptide (Dex-), as this is an MHC-I Dextramer. Approximately 10 % of the CD4 T cells were found in the vasculature (IV+). These results suggest that circulating OVA-specific CD8 T cells get activated in an antigen-dependent fashion and transmigrate across the BBB where they reside in the parenchyma.

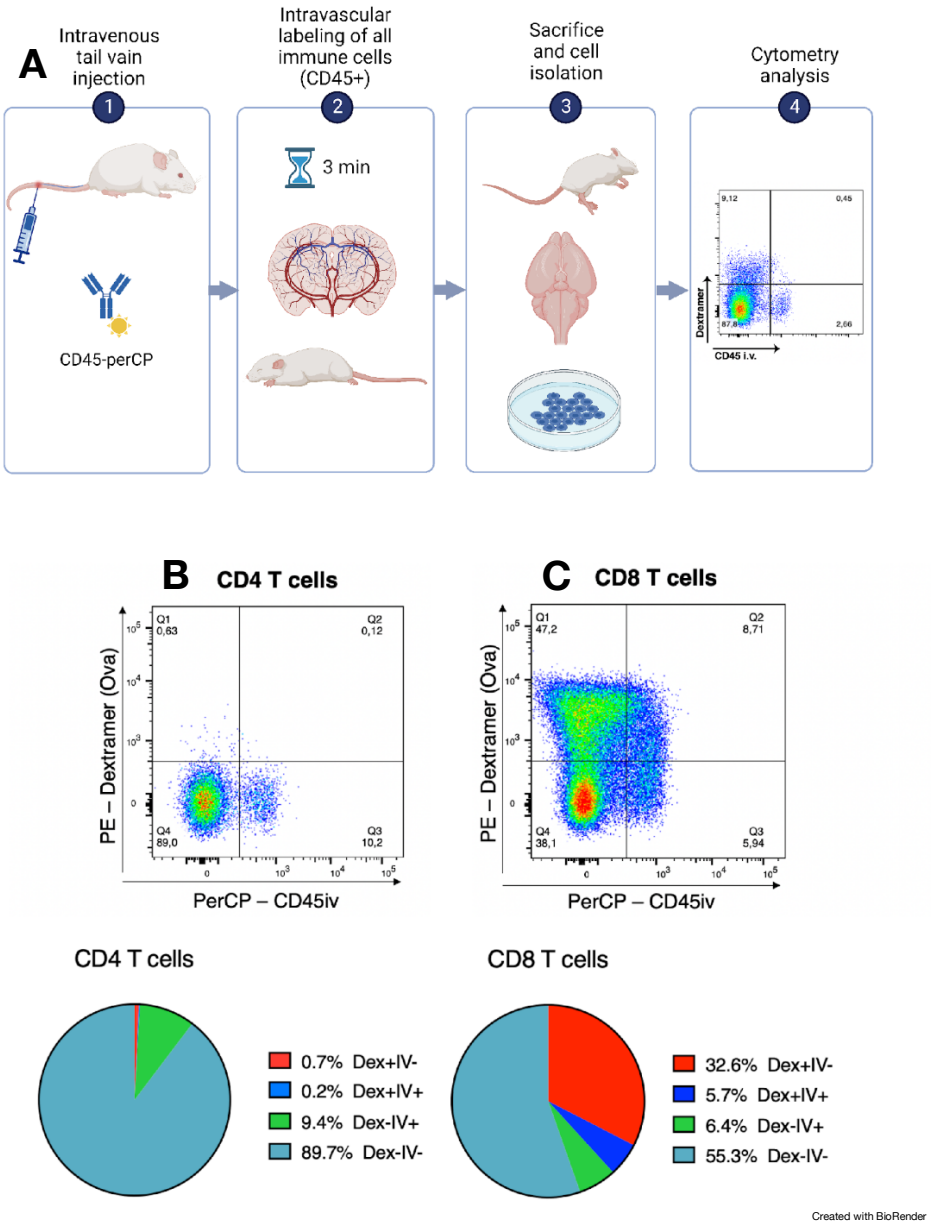

Figure 7: Differentiation of T cells into intravascular and parenchymal subpopulations.

(A) Setup for intravenous CD45 positive immune cell labeling. (B) Flow cytometer gating example for intravascular (IV+) vs. PE-Dextramer ovalbumin (Dex+) CD4 T cells and a pie chart showing the mean percentage of CD4 T cell subpopulations regarding specificity for ovalbumin (Dex) and localization (IV=intravenous). (C) Flow cytometer gating example for intravascular (IV+) vs. PE-Dextramer ovalbumin (Dex+) CD8 T cells and a pie chart showing the mean percentage of CD8 T cell subpopulations regarding antigen specificity for ovalbumin (Dex) and localization (IV=intravenous).

3.1.3 Brain isolated immune cells show a cytokine expression profile of a cytotoxic T cell after in vitro ovalbumin peptide restimulation

To further characterize the T cell response in the brain of BrEndO mice, we analyzed the cytokine expression pattern of isolated immune cells. For this we cultured brain immune cells isolated from BrEndO mice in the presence or absence of 1 µM SIINFEKL peptide in vitro overnight (Figure 8A). A panel of 13 cytokines was measured using the Legendplex Th cytokine detection assay. The beads were measured with a flow cytometer and quantitated with the LEGENDplex software.

Figure 8B shows the concentration of five detected cytokines: interferon g (IFNg), interleukin 6 (IL-6), interleukin 17A (IL-17A), interleukin 13 (IL-13) and interleukin 10 (IL-10) with or without SIINFEKL restimulation. Interestingly, the concentration of IFNg increased from a baseline of around 1000 pg/ml to more than 15000 pg/ml. IL-6 and IL-10 were the second and third most abundant cytokines, however, their expression was not significantly influenced by restimulation with SIINFEKL peptide. IL17A and IL13 were detectable at low concentration in the unstimulated sample. Interestingly, SIINFEKL restimulation significantly increased the concentration of both IL-17A and IL-13 in the supernatant. These results indicate that immune cells isolated from the brain of BrEndO mice actively produce cytokines such as IFNg and IL-6. The 10-fold increase of IFNg after SIINFEKL stimulation suggests OVA-specific CD8 T cells as the main source of IFNg.

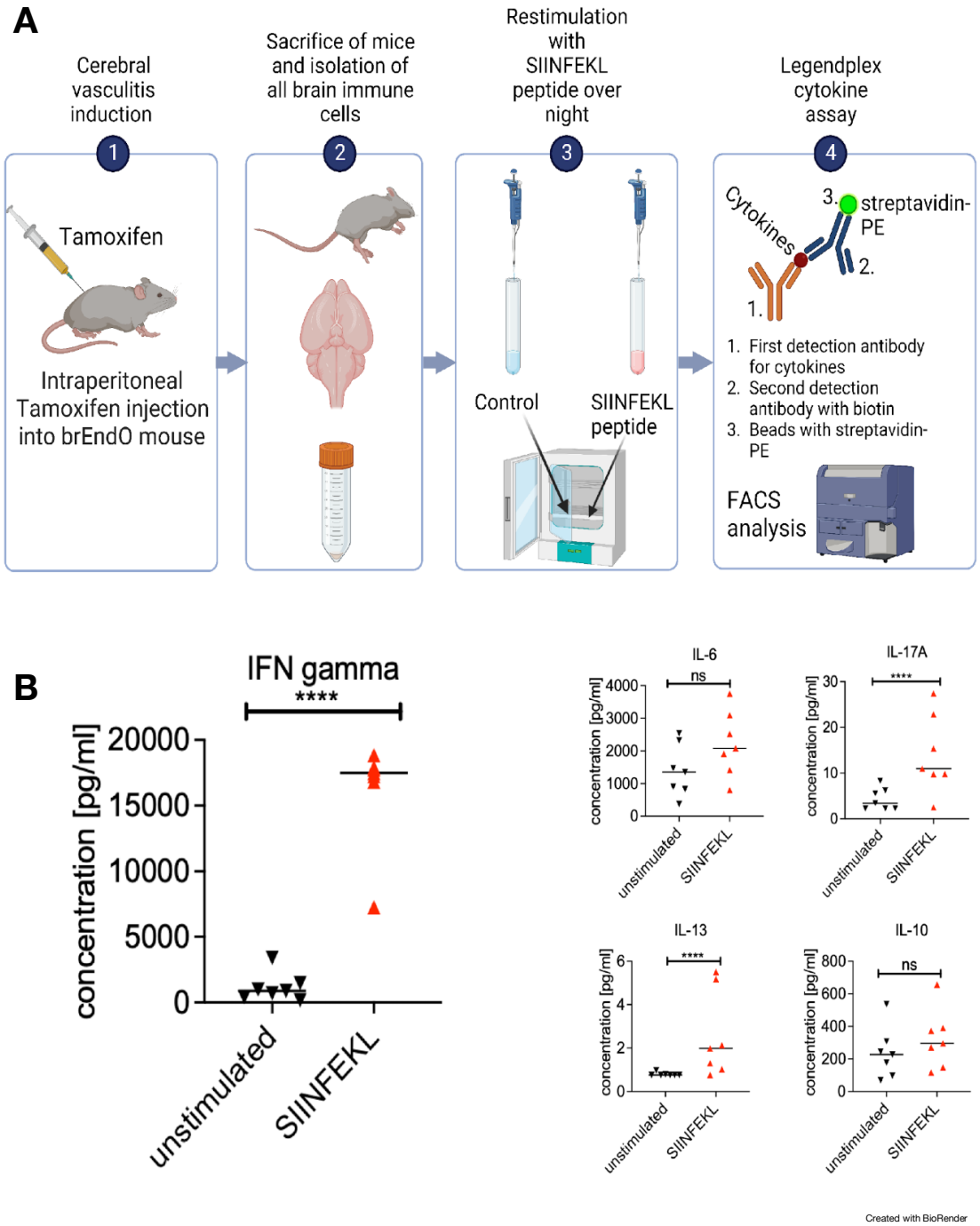

Figure 8: Legendplex cytokine assay with SIINFEKL peptide (OT-I) restimulation of immune cells isolated from a BrEndO mouse brain. (A) Experiment scheme of the SIINFEKL restimulation protocol and Legendplex cytokine assay principle (B) The concentration of IFNg after SIINFEKL stimulation increased 10-fold. The concentration of IL-6 after OT-I peptide stimulation did not increase significantly after SIINFEKL peptide stimulation. The concentrations of IL-17A and IL-13 increased significantly on a low level after SIINFEKL restimulation. The concentration of IL-10 did not increase after SIINFEKL restimulation.

* P ≤ 0.05. by students t-test

3.1.4 SIINFEKL-specific CD8 T cells from the brain of BrEndO mice express high level of CD39 and CXCR6 at day 11 and day 25.

We analyzed CD8 T cells derived from the brains of two distinct BrEndO mouse cohorts, towards the expression of CD39, P2X7 and CXCR6 on day 11 or day 25 after OVA induction. Using flow cytometry, we assessed the expression levels of the afore mentioned molecules on SIINFEKL-dextramer specific (Dex+) and other (Dex-) CD8 T cells. The left side of figure 9 displays exemplary histogram plots depicting the expression of these three specific markers on parenchymal CD8 T cells. Of note, Dex- cells are represented in blue, while Dex+ cells are highlighted in red. The right side of figure 9 presents overall statistical comparisons for Dex+ CD8 T cells (in red) and Dex- CD8 T cells (in blue) regarding the mean fluorescence intensity of CD39, P2X7 and CXCR6 on day 11 versus day 25.

SIINFEKL-specific (Dex+) parenchymal CD8 T cells from BrEndO mice exhibit elevated CD39 expression on day 11 compared to Dex-, which is further intensified by day 25 (Figure 9A). On the contrary, SIINFEKL-unspecific (Dex-) parenchymal CD8 T cells do not exhibit an elevation in CD39.

A recent study had shown that ATP sensing via the P2X7 receptor enhances the generation of tissue-resident memory CD8 T cells by increasing their sensitivity to the cytokine TGF-β (Borges da Silva et al., 2020). Consequently, we assessed the P2X7 expression in BrEndo mice on Dex+ and Dex- CD8 T cells at both day 11 and day 25. Although the fluorescence signal from the P2X7 antibody was relatively low, it revealed a higher level of P2X7 expression on Dex- cells on day 25 compared to day 11. A similar trend of intensified P2X7 expression was observed in Dex+ CD8 T cells.

Finally, we analyzed the expression of CXCR6. CXCR6 has been described as a marker for “autoagressive" CD8 T cells that also express P2X7 in non-alcoholic steato hepatitis (Dudek et al., 2021). Similarly, as CD39, CXCR6 is already highly expressed on Dex+ CD8 T cells on day 11 further intensifying by day 25. We conclude that SIINFEKL-specific CD8 T cells exhibit elevated expression of the activation markers CD39 and CXCR6 with this intensity increasing in later stages of the disease.

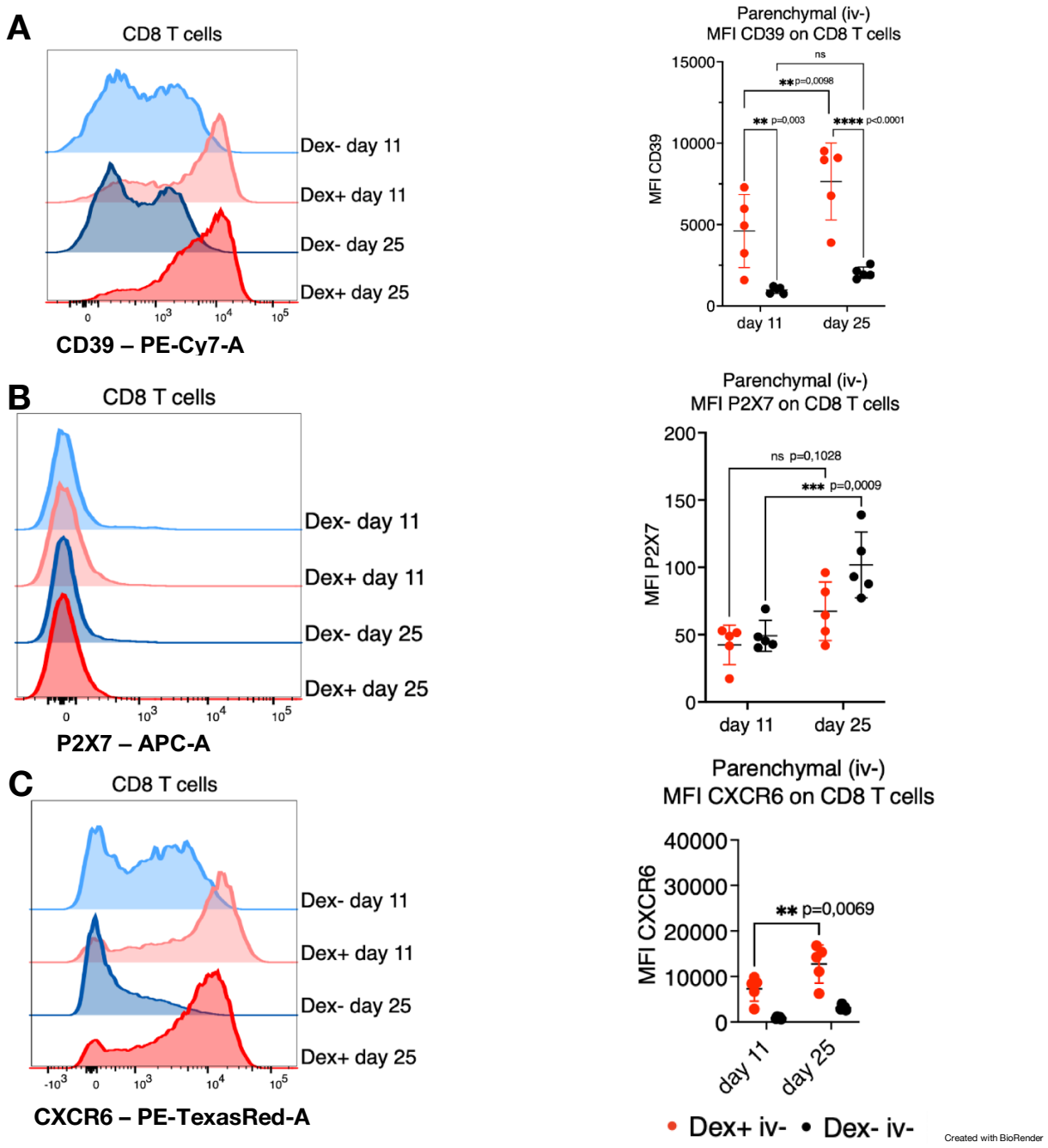

Figure 9: Subpopulations of cytotoxic T cells (CD8+) upregulate purinergic molecule expressions on day 25 compared to day 11 of BrEndO vasculitis. Flow cytometry derived exemplary histogram of the expression of (A) CD39, (B) P2X7 and (C) CXCR6 on SIINFEK-specific (Dex+) and other (Dex-) CD8 T cell populations from the brain of BrEndO mice on day 11 and day 25 of the experiment. n=5 for each mouse cohort, * $p \leq 0.05$. by two-way ANOVA, ** $p \leq 0.005$ and *** $p \leq 0.0005$

3.1.5 *In vitro* activated OT-I T cells upregulate *P2rx7* mRNA when arriving at the BBB.

In tamoxifen-activated BrEndO mice, priming of CD8 T cells on SIINFEKL-expressing brain endothelial cells might not result in the full activation of SIINFEKL-specific CD8 T cells. Taking this into consideration, we devised an alternative experimental setup. In this setup, SIINFEKL-specific CD8 T cells isolated from OT-I mice were activated *in vitro* by OT-I peptide stimulation and subsequently transferred into Tamoxifen-treated BrEndO mice (see Figure 10A). Tamoxifen injections were administered from day 1 to day 3. On day 4, we sacrificed an OT-I mouse and stimulated its splenocytes with 1 µM SIINFEKL peptide in a petri dish at 37°C overnight. On day 5, the splenocytes were collected and intraperitoneally injected into Tamoxifen-treated BrEndO mice or Cre- control mice. Finally, on day 11, we sacrificed the mice, isolating brain OT-I T cells for further analysis.

Notably, OT-I treated BrEndO mice exhibited a progressive loss of body weight from day 9 onwards, while Cre- control mice maintained a stable body weight. The weight loss in Cre+ BrEndO mice was accompanied by reduced activity and neurological symptoms in some instances. Consequently, soft food and pain medication were administered from day 9 onwards (refer to figure 10B). Given the escalating weight loss in most mice, a majority had to be sacrificed before day 14, as indicated by the Kaplan-Meier survival curve in figure 10C. The transferred OT-I CD8 T cells, congenically marked with CD90.1, enabled tracking in BrEndO recipient mice, facilitating their isolation at the experiment's conclusion. This allowed us to compare mRNA from OT-I T cells isolated from the brains of BrEndO mice post-transfer to mRNA from OT-I T cells isolated immediately after *in vitro* SIINFEKL stimulation. We performed this comparison by qPCR, focusing on *P2rx7* mRNA levels (see figure 10D). Remarkably, *P2rx7* mRNA levels were 4-fold higher in OT-I T cells from the BrEndO mouse brain

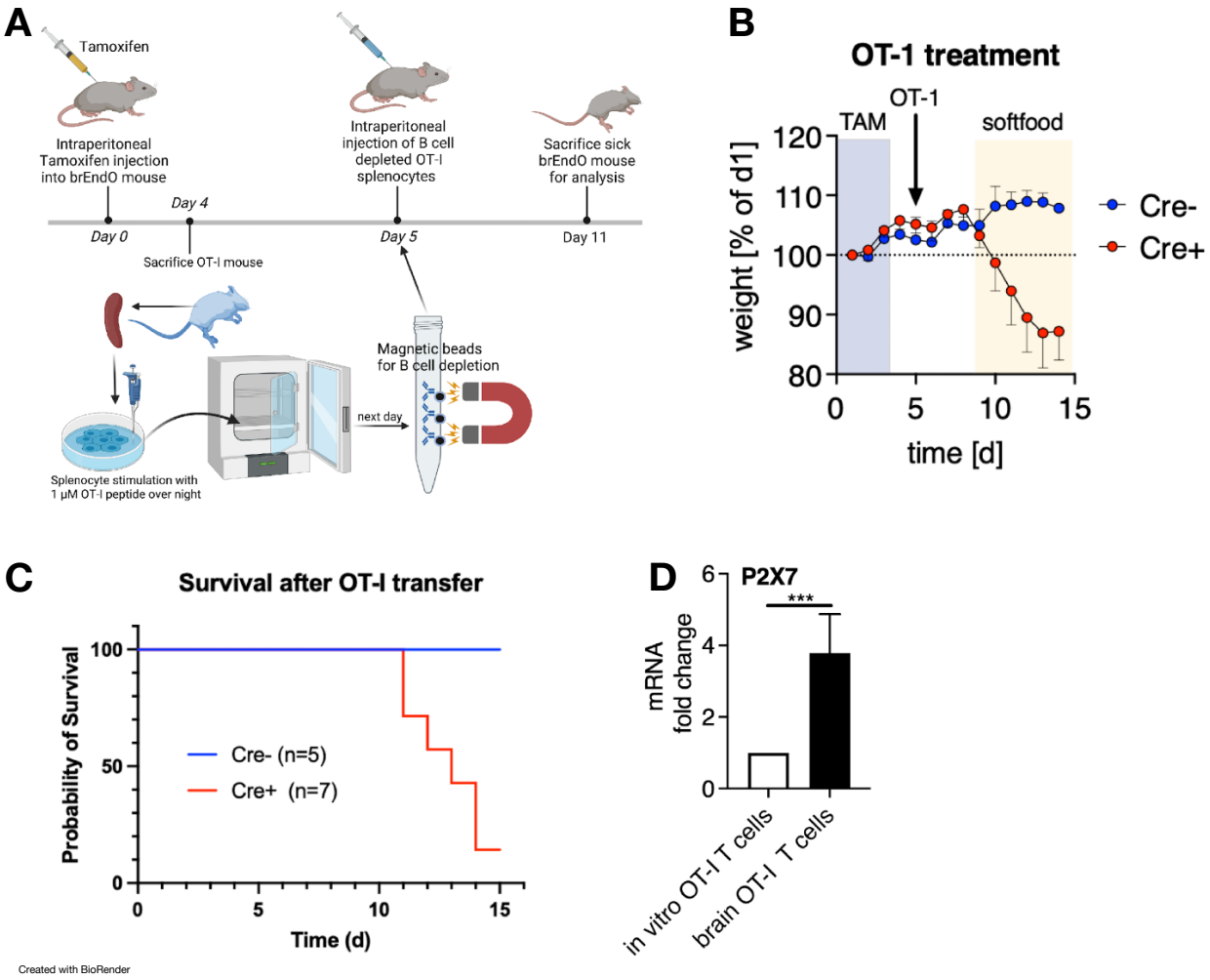

Figure 10: Ovalbumin specific T cell transfer (OT-I transfer) exacerbates the disease course of endogenous BrEndO mice. (A) Experimental setup for in vitro SIINFEKL peptide stimulation of OT-I T cells and transfer into BrEndO mice. (B) Weight curve comparing BrEndO vasculitis mice (Cre+) vs. control (Cre-) regarding their weight percentage of day 1 after OT-I T cell transfer on day 5. (C) Kaplan-Meier survival plot of BrEndO vasculitis mice (Cre+) after OT-I transfer on day 5. (D) qPCR data shows an increased P2rx7 mRNA expression of in vivo OT-I T cells taken from the BrEndO vasculitis mouse brain compared to spleen derived and in vitro overnight SIINFEKL-stimulated OT-I T cells.

* $p \leq 0.05$. by Students t-test, ** $p \leq 0.005$ and *** $p \leq 0.0005$

3.1.6 The cerebral microvessel transcriptome in BrEndO mice reveals an upregulation of purinergic pathway components

In the BrEndO mouse model, anti-OVA CD8 T cells target cerebral endothelial cells expressing and presenting OVA-derived peptides in MHC-I. This action induces inflammation in the immediate vicinity of affected brain blood vessels,

potentially leading to the release of purinergic molecules, such as ATP, serving as danger-associated molecular patterns (DAMPs). Our hypothesis posited that endothelial cells might leverage intrinsic purinergic pathways to mitigate inflammation and reinforce blood-brain barrier integrity (Gerasimovskaya and Kaczmarek, 2010).

To explore this, we extracted RNA from cerebral microvessels of Cre+ BrEndO mice isolated at days 11 and 32, as well as from Cre- control mice at day 11, and subjected it to mRNA sequencing. Initially, a comparison was made between Cre+ BrEndO mice and Cre- control mice on day 11, focusing on the expression of vessel cell type-specific genes. This analysis sought to detect potential "contamination" due to infiltrating immune cells during vasculitis, as illustrated in Figure 11A. Differentiation markers were used to identify immune cells associated with blood vessels, sourced from a study on vessel-associated immune cells in cerebrovascular diseases (Koizumi et al., 2019). Notably, the tight junction protein Cldn5, derived from brain endothelial cells, exhibited one of the highest mRNA levels, close to 10^4 transcripts per million (TPM). Additionally, other endothelial and astrocyte genes, such as Cdh5 for endothelial cells and Aqp4 for astrocytes, were highly abundant. Remarkably, both Cre+ BrEndO mice and Cre- control mice demonstrated similar expression levels of lineage marker genes for microglia, neurons, astrocytes, and endothelial cells. However, this similarity was not observed when examining immune cell-specific marker genes. Notably, Cre+ BrEndO mice exhibited a marked enrichment of lymphocytes compared to Cre- control mice. Specifically, mRNA sequences characteristic of T cells (CD3e, CD8a) and NK cells (Xcl1) were prominently elevated. This suggests that vessels isolated from Cre+ BrEndO mice contain a substantial number of immune cells, contributing the bulk mRNA used for sequencing.

Next, we compared the mRNA expression levels of essential purinergic components, including all P2X, P2Y, and P1 receptors, as well as nucleotide-degrading ecto-enzymes, between Cre+ BrEndO mice and Cre- control mice on day 11 (see Figure 11B). We found that the microvessel mRNA of Cre+ BrEndO mice had a significantly increased amount of mRNA encoding for the T cell ecto-ADP-ribosyltransferase ARTC2.2 (*Art2b*) and adenosine deaminase (*Ada*) along

with adenosine receptors 2a and 3 mRNA (*Adora2a* and *Adora3*), when compared to mRNA of Cre- mice. Among P2 receptor encoding, *P2rx4* mRNA expression was higher in Cre+ BrEndO mice compared to Cre- control mice on

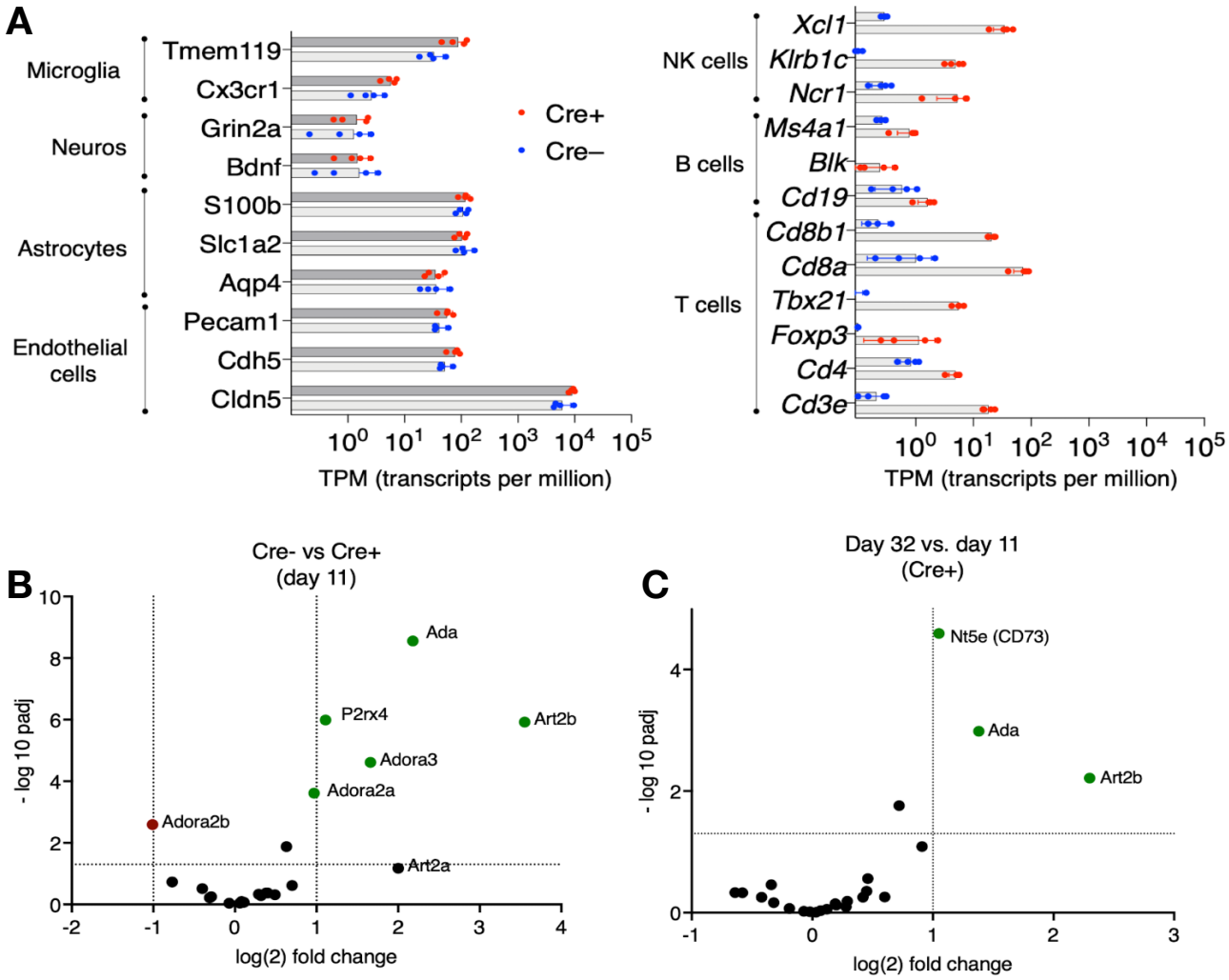

Figure 11: Modulation of purinergic mRNA expression in cerebral micro vessels across three groups of BrEndO vasculitis. (A) Microvessels exhibit distinctive mRNA sequences for microglia, neurons, astrocytes, endothelial cells, NK cells, B cells, and T cells. (B) Volcano plot presenting purinergic mRNA sequencing data, comparing the transcriptome of BrEndO mice on day 11 (Cre+) with control (Cre-). (C) Volcano plot illustrating purinergic mRNA sequencing data, comparing the transcriptome of BrEndO mice on day 11 vs. day 32.

Analyzed purinergic genes include Ada, Adora1, Adora2a, Adora2b, Adora3, Art2a, Art2b, Art3, Cd38, Enpp1, Entpd1, Nt5e, P2rx1, P2rx2, P2rx3, P2rx4, P2rx5, P2rx6, P2rx7, P2ry1, P2ry2, P2ry12, P2ry13, P2ry14.

n=4 for each analyzed BrEndO mouse group

day 11. Conversely, the expression of *Adora2b* was decreased in Cre+ BrEndO mice compared to Cre- control mice on day 11.

Furthermore, when comparing mRNA levels of Cre+ BrEndO mice isolated on day 11 and day 32, we observed significant changes as depicted in figure 11C. Specifically, the mRNA encoding for the adenosine-generating ecto-enzyme CD73 (*Nt5e*) was notably higher at day 32 compared to day 11. Additionally, the expression of *Ada* and *Art2b* mRNA was further increased from day 11 to day 32. To conclude, microvessel mRNA isolated from BrEndO mice contains a significant amount of leukocyte-derived mRNA as revealed by the comparison of Cre+ and Cre- mice at day 11, therefore, it is difficult to attribute the differential mRNA expression of purinergic receptors and/or ecto-enzymes to cells of microvessel e.g. endothelial cells.

3.2 Analyzing the impact of P2X7 antagonism in the BrEndO mouse model

3.2.1 Preliminary functional testing of the 13A7 nanobody demonstrates robust P2X7 inhibition on CD8 T cells in vitro

As depicted in figure 12A, the activation of the P2X7 receptor by ATP initiates the appearance and activation of metalloproteases ADAM 10 and ADAM 17 (TACE, TNF-α converting enzyme) at the cell surface, leading to the shedding of cell surface ecto-domains, including CD27. This process occurs within seconds of P2X7 activation (Moon et al., 2006, Safya et al., 2018). To assess the functionality of the produced 13A7 nanobodies, CD27 shedding in response to ATP stimulation was analyzed by real-time flow cytometry for quality control (Veltkamp et al., 2022). The analysis involved monitoring CD27 on 13A7 treated cells and cells treated with the control nanobody for 60 seconds. Subsequently, 300 µM ATP was added, and the measurement continued for 8 minutes. Notably, 300 µM of ATP was sufficient to activate P2X7 on cells treated with the control nanobody, resulting in a reduced mean fluorescence intensity (MFI) of CD27 as it was shed from the cell surface. In contrast, 13A7 treated cells exhibited only a slight decrease in CD27 MFI, indicating the functional efficacy of the produced 13A7 nanobody (depicted in Figure 12B).

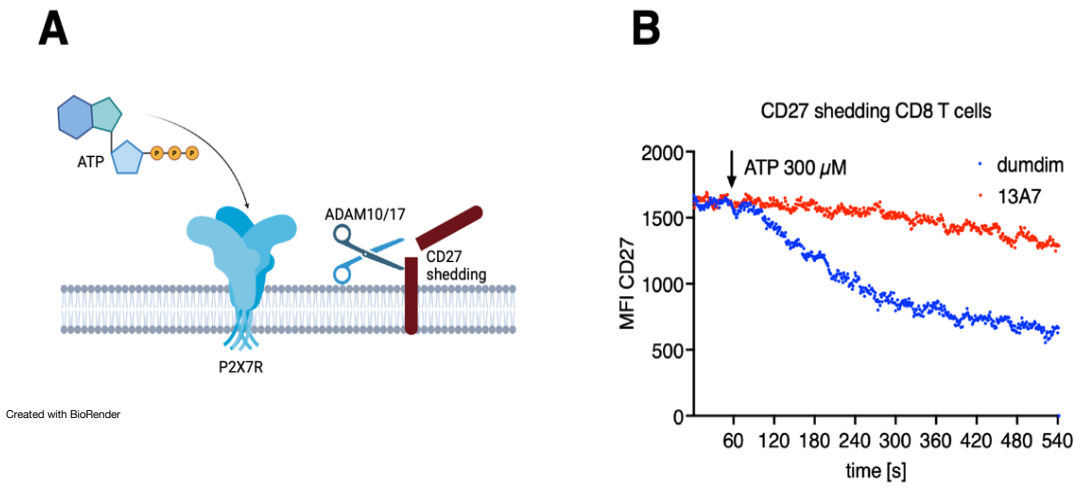

Figure 12: Functional testing of the 13A7 nanobody demonstrates robust P2X7 inhibition on CD8 T cells in vitro. (A) Schematic representation demonstrating proportional CD27 shedding downstream of ATP-gated P2X7 activation. (B) Changes in the mean fluorescence intensity of CD27 on CD8 T cells in vitro subjected to control nanobody (in blue) versus P2X7 inhibiting 13A7 nanobody (in red) after treatment with 300 µM ATP at the 60 second mark.

3.2.2 *13A7* nanobody treatment reduces the infiltration of CD8 T cells into the brain of BrEndO mice.

In section 3.1, our findings revealed a notable increase in *P2rx7* mRNA expression specifically in cytotoxic T cells isolated from the inflamed BrEndO brain. This, together with the impact of P2X7 blockade in other T cell-driven mouse models such as contact dermatitis (Danquah et al 2016), led to the hypothesis that the P2X7 receptor might contribute to cytotoxic T cells activation at the BBB in the BrEndO mouse model. To further investigate this hypothesis, a targeted pharmacological intervention was initiated by employing the inhibitory P2X7 nanobody clone 13A7 in the context of BrEndO vasculitis.

Figure 13A shows the three steps to produce the inhibitory P2X7 nanobody 13A7 and a non-binding control nanobody in a half-life extended format containing two 13A7 or control nanobodies linked to one nanobody that binds to albumin. In the initial step, HEK-6E cells were transfected with a plasmid encoding the sequence for the 13A7 or the control nanobody. Following a 6-day incubation period, the nanobodies were harvested and purified using a protein purification column as the second step. Subsequently, the third step involved running an SDS-PAGE gel with the flowthroughs from each protein purification step to assess any

potential protein loss. Additionally, we estimated the size and amount of the produced nanobodies by comparing them with the protein size ruler on the SDS-PAGE gel. After determining the protein concentration of the produced nanobodies by BSA assay, a quality control was performed.

For *in vivo* application 80 µg of nanobody was dissolved in 100 µL PBS. 13A7 and the control nanobody was administered on days 1, 5, and 9 (Figure 13A). On day 11, the mice were sacrificed, and immune cells were isolated from their brains.

Comparison of the weight curve of BrEndO mice treated with either 13A7 or control in Figure 13B revealed a clear gap from day 9 on.

Turning attention to specific cell counts, Figure 13C illustrates that microglia, a crucial component of the immune system within the central nervous system, do not exhibit a significant changes in numbers after 13A7 treatment.

The analyses of all CD8 T cells reveal a significantly lower number of parenchymal (iv-, green) CD8 T cells in the 13A7 BrEndO mice when compared to the control group, whereas vascular (iv+, black) CD8 T cell numbers are comparable among both groups (Figure 13D).

Next, the number of SIINFEKL-specific (Dex+) CD8 T cells were compared. Though there was a tendency towards a lower number of Dex+ CD8 T cells in the 13A7 group, the difference to the control group did not reach significance. The number of the remaining CD8 T cells (Dex-) was, however, significantly lower in the 13A7 group when compared to the control group (Figure 13E). In conclusion, P2X7 blockade has a potential impact on the CD8 T cell response against OVA at the BBB. Further experiments should be conducted with larger cohorts to verify these first findings.

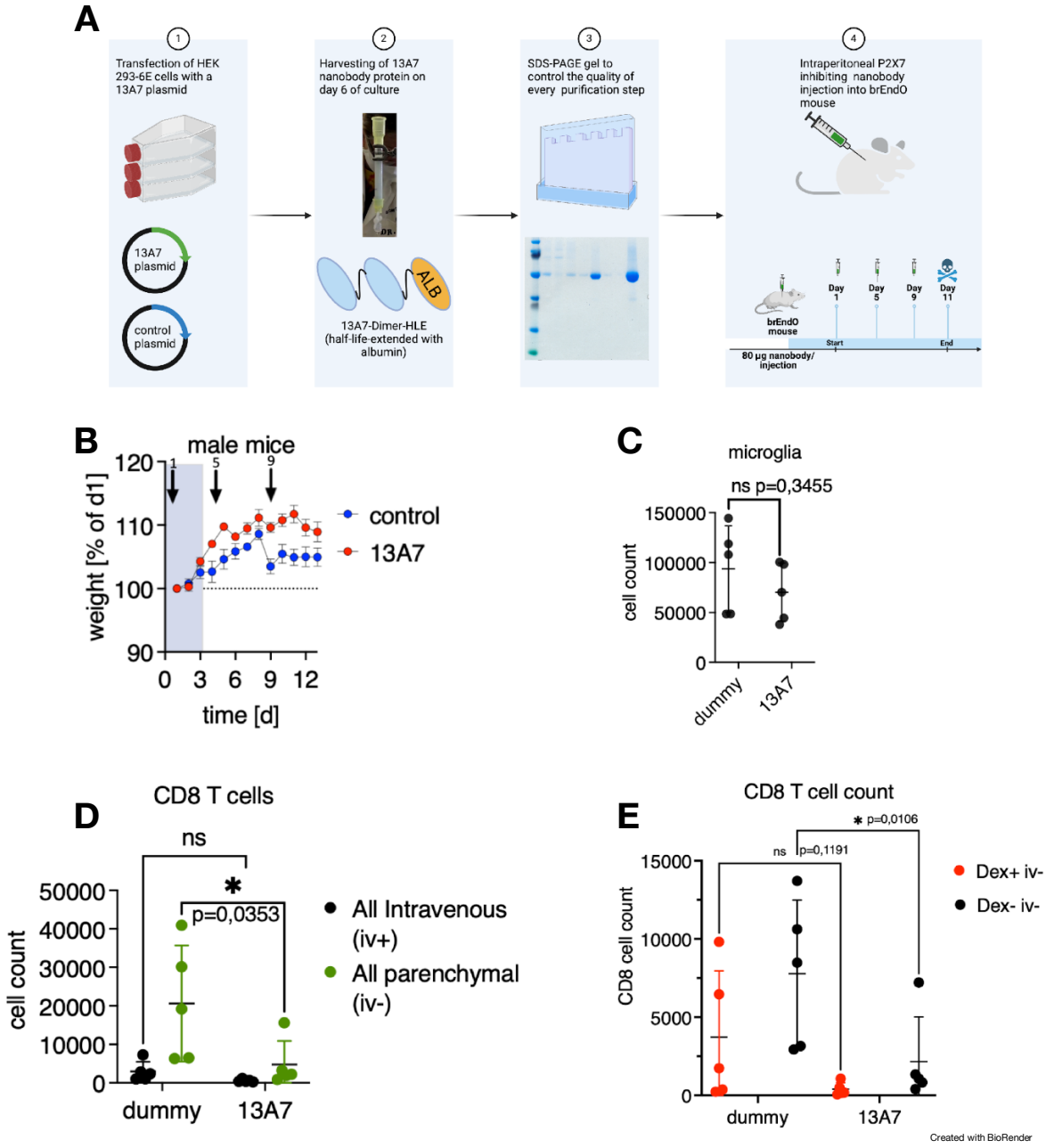

Figure 13: Subpopulations of CD8 T cells are reduced after P2X7 nanobody inhibition.

(A) Production of the inhibitory P2X7 nanobody 13A7, involving HEK293-6E cell transfection (1), nanobody protein purification (2), production control via SDS-PAGE gel (3), and intraperitoneal nanobody injection of 80 µg on day 1, 5 and 9. (B) Weight curve in percentage of day 1 comparing male BrEndO mice treated three times with a control nanobody dummy (in black) vs. 13A7 nanobody (in red) for 13 consecutive days. (C) The cell count of microglia is not significantly reduced after P2X7 nanobody blockade. (D) Overall, the cell count of all parenchymal CD8 T cells (in green) is diminished after P2X7 blockade. (E) The cell count of parenchymal CD8 T cells that are Dextramer- and iv- (in black) reduces. Dextramer+ and iv- CD8 T cells (in red) exhibit a tendency to decrease after P2X7 blockade.

* P ≤ 0.05 by two-way ANOVA

3.3 Establishing a lentiviral based genetic modification pipeline for purinergic ecto-enzyme expression in murine bEnd.3 cerebral endothelial cells

Previous research has highlighted variations in the expression of adenine nucleotide-degrading ecto-enzymes, such as CD73, between murine and human cerebral endothelial cells (Joolharzadeh and St Hilaire, 2019). Our objective was to establish a methodology for either genetically excising *Entpd1*/CD39 and CD38/*Cd38* or overexpressing the *Nt5e*/CD73 ecto-enzyme in the bEnd.3 mouse cerebral endothelial cell line.

Genetically modifying the bEnd.3 mouse cerebral endothelial cell line presents challenges, as past experiments unraveled that common transfection systems such as lipofectamine are unable to result in stable and high transfection rates in bEnd.3 cells (Dos Santos Rodrigues et al., 2019). However, synthesized liposomes conjugated to cell-penetrating peptides can overcome this limitation but are not publicly available yet (Dos Santos Rodrigues et al., 2019).

In this chapter, we introduce a comprehensive pipeline that combines a plasmid transfection method with a lentiviral transduction system developed by Dr. Riecken and coworkers (Weber et al., 2012, Cong and Zhang, 2015). This integrated approach ensures a stable transduction of cell lines, including bEnd.3 cells, addressing the limitations encountered by conventional transfection methods.

3.3.1 Generation of CD73-overexpressing bEnd.3 cells

In contrast to human brain endothelial cells, primary murine brain endothelial cells as well as immortalized bEnd.3 cells lack CD73 expression. Therefore, our objective was to introduce CD73 expression into bEnd.3 cells using the lentiviral transduction system described above.

Figure 14A outlines a 7-step process for generating bEnd.3 cells that overexpress CD73. In step 1, an *Nt5e* plasmid with restriction sites and an antibiotic resistance gene was ordered. Step 2 involved digesting the *Nt5e* plasmid and a Lentivirus plasmid backbone. Ligation of the plasmids occurred in step 3, followed by the transformation of the new plasmid into E. coli bacteria in step 4. After an overnight incubation, an E. coli growing on selection agar was selected in step 5 and subsequently amplified. Step 6 involved sequencing the amplified plasmids, and

once alignment was confirmed, they were sent to Dr. Riecken, an expert in lentiviral transduction at the University of Hamburg. In step 7, the plasmid was incorporated into a lentivirus, which was then used to transduce wildtype bEnd.3 cells. CD73 expression and eGFP reporter gene expression were assessed via flow cytometry. CD73high bEnd.3 cells were isolated via FACS and further cultured, establishing CD73high and CD73low bEnd.3 cells, as confirmed by flow cytometric analyses (Figure 14B). Notably, the eGFP reporter expression matched CD73 expression in these lines.

Functionality tests for CD73 in CD73low and CD73high bEnd.3 lines involved measuring their capacity to degrade extracellular AMP. Utilizing the luciferase-based AMP Glo assay, wildtype bEnd.3, CD73low, and CD73high bEnd.3 lines were incubated with 10 µM AMP for 40 minutes. The luminescence signal significantly decreased in CD73low and CD73high bEnd.3 cells when incubated with 10 µM AMP, indicating the presence of functional CD73 (Figure 14C). In contrast, wildtype bEnd.3 cells showed a high luminescence signal, confirming their inability to degrade AMP to adenosine.

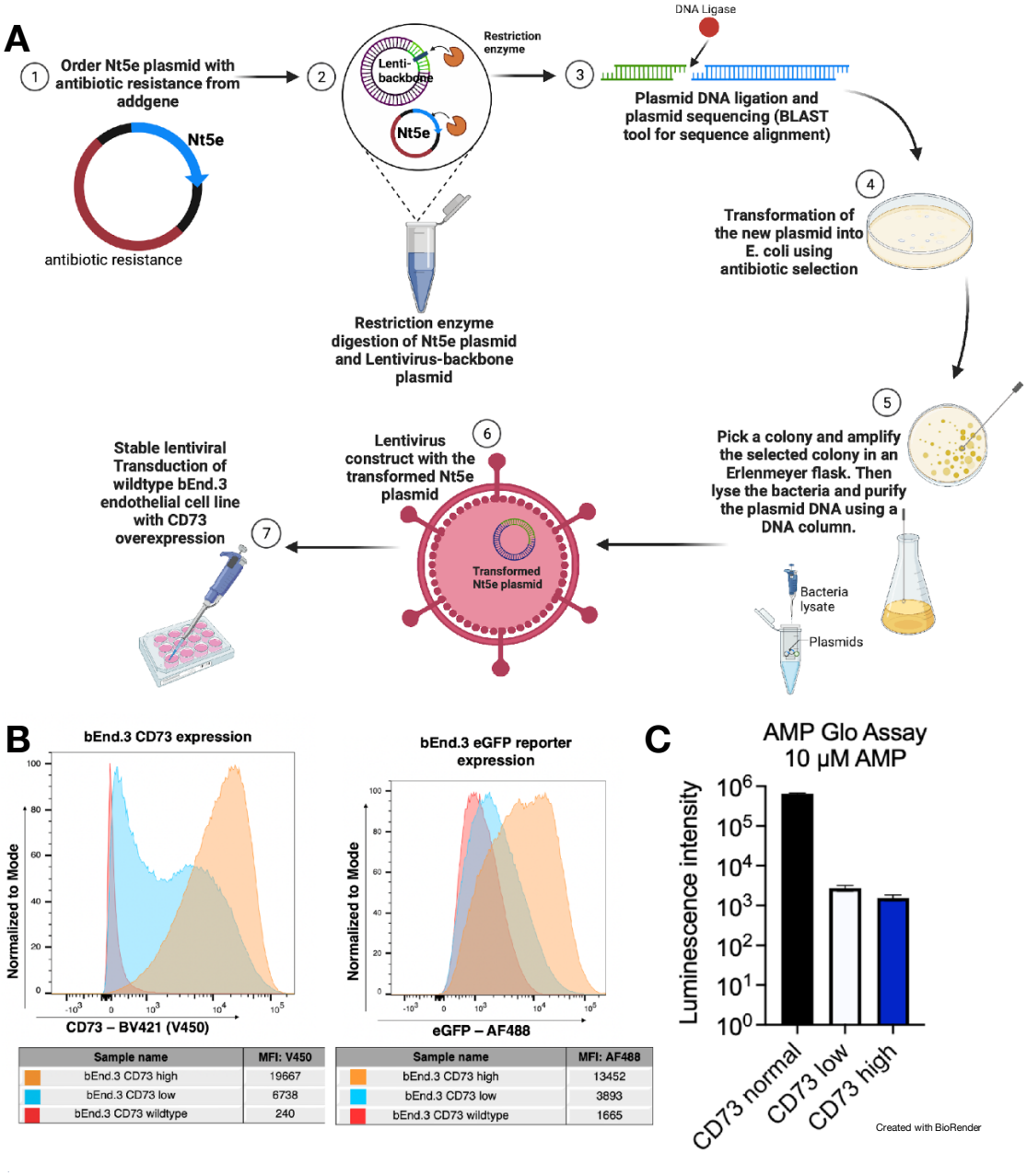

Figure 14: Establishing a mouse cerebral endothelial cell line (bEnd.3) with CD73 ecto-enzyme overexpression through stable lentiviral transduction. (A) Illustration of a pipeline for gene overexpression in bEnd.3 cerebral endothelial cells using a lentivirus construct. (B) Flow cytometer histogram analysis, depicting the correlation between CD73 expression levels and eGFP reporter expression in three transfected bEnd.3 cell lines, which were sorted for high or low CD73 expression, alongside wildtype CD73 expression. (C) Results from the AMP Glo Assay demonstrate that bEnd.3 cell lines with elevated CD73 expression exhibit a heightened functional enzymatic capacity to degrade AMP to adenosine, evidenced by a decrease in luminescence intensity.

3.3.2 Generation of CD39 and CD38 bEnd.3 knockout bEnd.3 cell lines

The 7-step pipeline detailed in section 3.3.1 was applied to generate two novel bEnd.3 cell lines, each featuring a knockout for either *Entpd1* (CD39) or *Cd38* (CD38) using the CRISPR/Cas9 system. To design guide DNA sequences for *Entpd1* and *Cd38* with the highest probability for gene knockout and minimal off-target binding, the CHOPCHOP tool website was employed (Labun et al., 2019). A distinct lentivirus backbone plasmid, incorporating the Cas9 gene and the new guide DNA sequences for *Entpd1* and *Cd38*, was employed. To obtain the knockout bEnd.3 cell lines, we utilized an mCherry reporter system from the lentivirus vector and subjected the bEnd.3 cells to multiple FACS-based sorting processes after successful transfection. In figure 15A, histograms illustrate the successful knockout of *CD38*, showcasing a reduced mean fluorescence intensity of 2068 after CD38 knockout, as opposed to 13717 in the wildtype bEnd.3 cell line. Additionally, we observed an increase in mCherry reporter expression to a mean fluorescence intensity of 5298 in the CD38 knockout compared to 2153 in the CD38 wildtype bEnd.3 cell line. Furthermore, figure 15B presents histograms depicting the mean fluorescence intensity of CD39 knockout bEnd.3 cells, which decreased to 362 compared to 3930 in the bEnd.3 wildtype

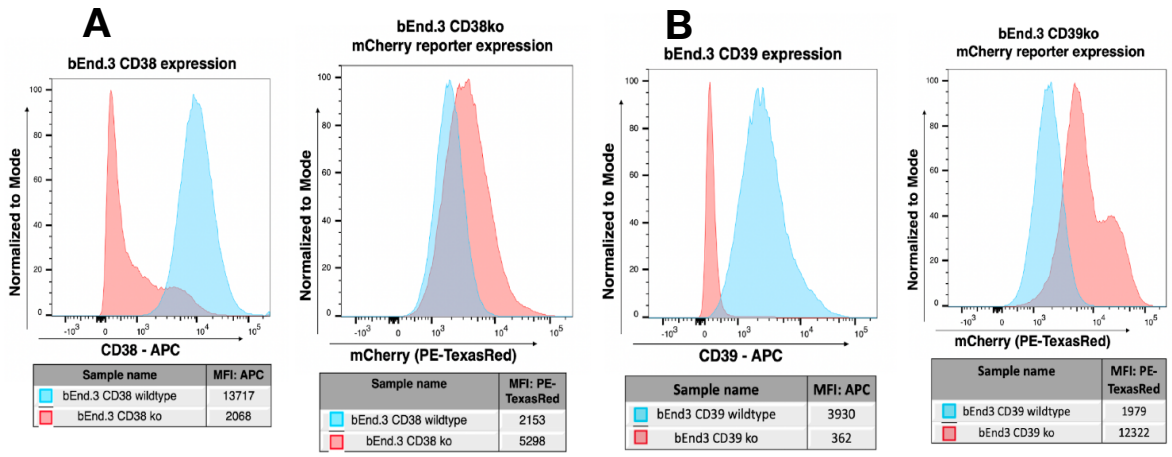

Figure 15: Generation of two mouse cerebral endothelial cell lines (bEnd.3) with a knockout for either CD39 or CD38 using stable lentiviral transduction. (A) Flow cytometry analyses generated histograms comparing the CD38 deficient bEnd.3 cell line (in red) and the CD38 wildtype cell line (in blue) in concordance with the PE-TexasRed reporter gene expression, which represents successful lentiviral transduction in the bEnd.3 CD38 knockout cell line. (B) Flow cytometer histogram comparison of the CD39 deficient bEnd.3 cell line (in red) and the CD39 wildtype cell line (in blue) in concordance with the PE-TexasRed reporter gene expression, which represents successful lentiviral transduction in the bEnd.3 CD39 knockout cell line.

cell line. Conversely, the mCherry reporter expression of the lentiviral backbone plasmid increased to a mean fluorescence intensity of 12322 compared to 1979 in the bEnd.3 wildtype cell line. These newly established bEnd.3 lines can be further characterized in the future towards their capacity to generate ADP-ribose from nicotinamide adenine dinucleotide in the case of CD38 knockout bEnd.3 or ADP/AMP from ATP in the case of CD39 knockout bEnd.3.

4. Discussion

The experiments performed as part for this medical doctoral thesis yielded the following major new findings:

(1) CD8 T cells specific to SIINFEKL presented in MHC-I infiltrate the brain parenchyma of BrEndO mice, from where they target cerebral endothelial cells.

(2) Brain-infiltrating SIINFEKL-specific CD8 T cells exhibit a high expression of CXCR6 and CD39, further increasing in late stages of BrEndO vasculitis.

(3) Pharmacological inhibition of the ATP-gated purinergic receptor P2X7 reduces the invasion of CD8 T cells into the brain parenchyma of BrEndO mice.

(4) mRNA isolated from microvessels of BrEndO mice contains a significant amount of leukocyte-derived mRNA making it difficult to attribute the differential mRNA expression of purinergic receptors and/or ecto-enzymes to cells of microvessel e.g. endothelial cells.

(5) The murine cerebral endothelial bEnd.3 cell line can be genetically modified through lentiviral transduction to resemble the expression pattern of purinergic ecto-enzymes typically observed in humans.

4.1 CD8 T cells are key players in the cerebral endothelial BrEndO mouse model

The immunopathology of Primary Angiitis of the Central Nervous System (PACNS) remains only partially understood. In contrast to giant cell arteritis, human PACNS exhibits a predominant presence of CD8 T cells and macrophages in late activation stages (Mihm et al., 2014).

Using intravascular immune cell staining in our BrEndO mouse model, we also observed predominant SIINFEKL/MHC-I specific CD8 T cells infiltrating the brain parenchyma and targeting cerebral endothelial cells (see section 3.1). Mechanistically, it is yet unclear whether the CD8 T cells are primed by cerebral endothelial cells acting as semi-professional antigen-presenting cells, or by dendritic cells, which take up ovalbumin peptides and activate CD8 T cells (Epperson and Pober, 1994). However, endothelial cells are sentinels of the immune system capable of activating CD8 T cells and accelerating tissue infiltration (Mai et al., 2013, Amersfoort et al., 2022). As OVA is exclusively expressed in endothelial cells of brain microvessels – due to the Slco1c1-Cre in the BrEndO mouse – presentation of SIINFEKL on MHC-I is confined to brain

endothelial cells in theory. Interestingly, the CD8 T cell response against OVA-derived antigens triggered in BrEndO mice seems to be of transient nature (unpublished observation of the research group). In contrast to the OT-I transfer model into the BrEndO mouse, which results in mostly fatal outcome (see 3.1.5), the immune response in the endogenous BrEndO model against SIINFEKL/MHC-I resolves 5-6 weeks after tamoxifen injection, although OVA is still expressed at the BBB (unpublished observation of the research group).
In the absence of an inflammatory milieu, the sole expression of OVA in cerebral endothelial cells might induce only an incomplete priming or spontaneous tolerization of SIINFEKL-specific CD8 T cells, resulting in mild vessel injury (Certo et al., 2021, Hargadon et al., 2006, Busselaar et al., 2020). However, already in vitro primed OT-1 T cells transferred into a BrEndO mouse lead to severe vessel damage, which is probably caused by a directly targeting cerebral endothelial cells. Therefore, therapeutic strategies focusing on tolerogenic cross-presentation of foreign antigens via nanoparticles to endothelial cells could be a promising approach for treating CD8 T cell-driven autoimmune diseases, if the autoantigen is known (Carambia et al., 2021).

However, we cannot rule out the involvement of other classical antigen presenting cells like dendritic cells in the initiation of the immune response. Dendritic cells might take up full length OVA or OVA-derived peptides (e.g. SIINFEKL) from damaged cerebral endothelial cells and cross present them to CD8 T cells (Fu and Jiang, 2018). The impact of dendritic cells that cross present OVA peptides could be investigated in BrEndO mice in the future.

4.2 SIINFEKL specific intraparenchymal CD8 T cells upregulate CXCR6 and CD39 in late stages of BrEndO mice

In our endogenous BrEndO model, SIINFEKL specific, parenchymal CD8 T cells show an increased expression of chemokine receptor 6 (CXCR6) and ecto-nucleotidase CD39 on day 25 compared to the clinical peak of the disease on day 11.
In general, CXCR6 plays a key role in directing tissue-resident memory CD8 T cells (T_{RM} CD8 T cells) to specific tissues, such as the airways (Wein et al., 2019).

Recently, this has also been demonstrated in the context of Alzheimer's disease, where CD8 T cells upregulate CXCR6 to orchestrate residency and interact with microglia, thereby reducing proinflammatory cytokine production and restricting the pathology of Alzheimer's disease (Su et al., 2023). Intriguingly, also patients with neuroinflammatory diseases such as multiple sclerosis or neurodegenerative diseases show an increased density of CD8 T_{RM} cells in the central nervous system compared to healthy controls (Merkler et al., 2022). In MS, these T_{RM} CD8 T cells appear in demyelinating lesions and in normal-appearing white matter close to blood vessels (Vincenti et al., 2022). In line with that, several cancers induce upregulation of CXCR6 on CD8 T_{RM}, which directs them into perivascular niches of the tumor stroma to interact with CXCR6 ligand-positive dendritic cells for a potent anti-tumor immune response (Mabrouk et al., 2022).
Overall, tissue-resident memory CD8 T cells are a subset of memory CD8 T cells that retain the ability to persist in tissues long-term after an initial infection or immunization (Mueller and Mackay, 2016). Compared to central memory and effector memory T cells, T_{RM} CD8 T cells proliferate locally in non-lymphoid tissues, provide local immune surveillance, and rapidly protect against viral re-infection (Vincenti et al., 2022).

The observed increase of CD39 expression on intraparenchymal, antigen specific CD8 T cells in the BrEndO mouse model may indicate the regulatory process of switching off the immune response during the recovery from the disease (Timperi and Barnaba, 2021). Consistent upregulation of CD39 occurs upon CD8 T cell activation causing a decline in early effector function (Timperi and Barnaba, 2021). However, this upregulation contributes to a higher frequency of antigen specific CD8 T cells at later time points (Raczkowski et al., 2018).
Other studies described CD39 as a marker of exhausted, tumor-antigen specific CD8 T cells, which was associated with co-expression of CD103 in several cancer types (Duhen et al., 2018). CD103 is a prominent marker for tissue resident memory CD8 T cells and is associated with better survival in several cancer types (Timperi and Barnaba, 2021).

Consistent with our findings, a neuro-immunological study using a similar intravascular immune cell staining technique showed that peripheral virus infections induce brain tissue-resident memory CD8 T cells providing protection after murine CNS infection (Urban et al., 2020). This study adoptively transferred eGFP-expressing SIINFEKL specific CD8 T cells and infected the recipient mouse with a pathogen re-expressing the same SIINFEKL (Urban et al., 2020).
In another investigation on patients with subclinical neuroinflammation and a familial predisposition for multiple sclerosis (SCNI), tissue-resident memory CD8 T cells with a clonal expansion pattern were found (Beltran et al., 2019).

While not conclusive proof of tissue-resident memory T cells in BrEndO vasculitis mice, these observations may lead to further investigation of T cell memory development of antigen specific CD8 T cells (Mix and Harty, 2022).
Taken together, CD8 T_{RM} cells may develop during the late course of BrEndO vasculitis. Their CXCR6 expression may orchestrate residency and indicates a prolonged survival and an immunoregulatory role. The increase of CD39 expression may indicate CD8 T cell exhaustion, which could be associated with the development of CD8 T_{RM} cells.

4.3 Pharmacological inhibition of the purinergic ATP receptor P2X7 reduces CD8 T cell invasion into the brain.

Even though the ATP gated receptor P2X7 receptor is not highly expressed on T cells, it plays a crucial role in their function. This receptor, which is primarily known for its involvement in the immune response and inflammation, has been shown to influence T cell activity, survival, and differentiation (Grassi, 2020, Rivas-Yanez et al., 2020). Studies indicate that P2X7 activation can modulate T cell receptor signaling and cytokine production, thereby impacting the overall immune response (Grassi, 2020). For instance, it was demonstrated that ATP released through pannexin-1 hemichannels activated P2X7 receptors to enhance T cell activation and proliferation (Schenk et al., 2008). Subsequently, the P2X7 receptor is widely acknowledged as a therapeutic target in several T cell driven inflammatory diseases (Burnstock and Knight, 2018).

Regarding CD8 T cells, it was demonstrated that the P2X7 receptor imprints a pro-memory transcriptional signature (Vardam-Kaur et al., 2022). In line with that the P2X7 receptor increased the metabolic fitness of long-lived memory CD8 T cells (Borges da Silva et al., 2018). Further roles of P2X7 on CD8 T cells have mainly been studied in the context of tumor immunity. A study on tumor immunology in experimental melanoma found that P2X7 receptor knockout mice displayed a decreased tumor infiltration of CD8 T cells and increased infiltration of regulatory T cells (De Marchi et al., 2019).

In section 3.1.5, we demonstrate that *P2rx7* mRNA is upregulated on brain OT-1 T cells 6 days after adoptive transfer, when compared to OT-1 T cells directly before transfer. In addition, we found that P2X7 expression is higher on CD8 T cells isolated from BrEndO mice on day 25 when compared to CD8 T cells isolated on day 11 (see section 3.1.4). First, this suggests that the inflammation at the blood-brain-barrier in BrEndO mice impacts the level of P2X7 expression on CD8 T cells. Second, this raises the question whether targeting P2X7 could be a therapeutic option to treat cerebral vasculitis.
The 13A7 nanobody specifically inhibits P2X7 (Jank et al., 2019, Pinto, 2018, Danquah et al., 2016). As described in section 3.2, we injected 80 µg of the 13A7 nanobody on days 1, 5 and 9 of BrEndO vasculitis and observed a reduction of the total parenchymal CD8 T cells in the brain on day 11. This was accompanied by a tendency to prevent the typical weight drop of the BrEndO mice, which is a clinical hallmark of disease manifestation in the BrEndO mouse model. We conclude that P2X7 could have an impact on several stages of the BrEndO mouse model such as CD8 T cell priming, migration and effector function, which may aggravate cerebral vessel inflammation in BrEndO mice.

The P2X7 blockade related amelioration of the T cell driven vasculitis is in line with other preclinical mouse studies that observed reduced inflammation after P2X7 antagonism e.g. allergic contact dermatitis and experimental murine glomerulonephritis after pharmacological inhibition of P2X7 (Danquah et al., 2016, Taylor et al., 2009, Jank et al., 2019). Moreover, intracerebroventricular

injections of an anti-P2X7 nanobody into stroke mice with temporary cerebral artery occlusion reduced stroke lesions (Wilmes et al., 2022).

Future studies with the BrEndO mouse model should investigate a potential link of P2X7 expression and the development of tissue resident memory CD8 T cells. Sustained P2X7 receptor activation is necessary for the survival and mitochondrial fitness of memory CD8 T cells (Borges da Silva et al., 2018). P2X7 expression was found fundamental for the differentiation of memory CD8 T cells by means of the activation of the AMP kinase signaling pathway and promotion of mitochondrial function (Vardam-Kaur et al., 2022). In that study, P2X7 also promoted the upregulation of the TGF-b signaling pathway, which is crucial for epithelial resident memory T cell populations (Vardam-Kaur et al., 2022). Moreover, P2X7 expression was observed specifically strong on CXCR6+ tissue resident memory CD8 T cells in experimental non-alcoholic steatohepatitis (NASH). These liver T_{RM} CD8 T cells displayed an overshooting calcium influx which suggested the involvement of cation channels such as P2X7. Subsequent inhibition of the cation channels P2X7 or Pannexin 1 prevented auto-aggression by liver T_{RM} cells but sustained the physiological antigen-specific cytotoxicity (Dudek et al., 2021). As our current study lacks to draw a definite connection of tissue resident memory CD8 T cells and detrimental P2X7 signaling, further studies are needed to evaluate if P2X7 inhibition targets possibly detrimental CXCR6 positive tissue resident memory CD8 T cells in BrEndO mice. This finding would be of high interest, since generation of T_{RM} cells early in the life of mice predisposes to autoimmune diseases of the brain (Steinbach et al., 2019). Hence, inhibition of the purinergic P2X7 receptor on CD8 T cells may represent an interesting therapeutic target in cerebral vasculitis.

On a side note, P2X7 blockade could also impact myeloid cell populations, particularly microglia. Microglia rely on P2X7 for the release of pro-inflammatory cytokines and reactive oxygen species (Monif et al., 2009). Additionally, P2X7 signaling modulates clearance of extracellular debris by microglial cells as well as autophagy (Campagno and Mitchell, 2021). However, we observed no changes in the absolute cell count of microglia in the brain (see section 3.2).

Future research could investigate cytokine levels and phagocytic activity to further understand microglial involvement.

Cerebral endothelial cells also express P2X7, which affects blood-brain barrier (BBB) integrity and immune cell infiltration (Aslam et al., 2021, Ludewig et al., 2019). In myeloid cells, P2X7 activation triggers activation of the NLRP3 inflammasome, leading to the formation of Gasdermin D (GSDMD) pores in the plasma mebrane (Swanson et al., 2019). Recent studies have shown that nanobodies blocking the GSDMD in brain endothelial cells can preserve its integrity after lipopolysaccharide treatment (Wei et al., 2024) highlighting the importance of studying other pore-forming molecules such as P2X7. Furthermore, interactions between T cells and activated endothelial cells can prime T cells for tissue residency, potentially leading to harmful tissue-resident memory CD8 T cells (Wienke et al., 2022). Therefore, the role of P2X7 signaling in the interplay between cerebral endothelial cells and CD8 T cells in BrEndO remains a key area of interest.

In summary, the effects of P2X7 blockade on CD8 T cells, microglia, and cerebral endothelial cells underscore the potential of targeting P2X7 for managing neuroinflammatory conditions.

4.4 Microvessel-derived mRNAs encoding for proteins involved in purinergic signaling are differentially expressed during experimental cerebral vasculitis

As we observed that pharmacological inhibition of P2X7, a key player in purinergic signaling of immune cells, had an impact on the disease course, we performed bulk RNA sequencing of mRNA isolated from cerebral microvessels (Lee et al., 2019).

The mRNA sequencing revealed that the obtained microvessel mRNA contained a lot of “signature mRNAs” for infiltrating immune cells e.g. NK cells, B cells, and T cells (see figure 11). Thus, it is difficult to solely attribute changes in purinergic signaling mRNA expression level to vessel cells such as endothelial cells. In the future, single cell mRNA sequencing or single nuclei mRNA sequencing could

solve this problem (Czupalla et al., 2018). The latter could be more suitable as it is technically challenging to isolate single endothelial cells (Kimble et al., 2022).

In the mRNA sequencing data, we found an increased *P2rx4* expression in total microvessel mRNA of Cre(+) BrEndO mice at the peak of the disease on day 11 compared to Cre(–) control mice. Moreover, we found that the adenosine receptor *Adora2b* is downregulated, while *Adora2a* and *Adora 3* were upregulated in microvessels of Cre(+) BrEndO mice. Upon comparing the purinergic expression levels in BrEndO mice between day 11 and day 32, which corresponds to the recovery stage, we observed an upregulation of *Nt5e* and *Ada* mRNAs coding for the CD73 ecto-enzyme and the adenosine deaminase (ADA). On a side note, the highest fold change for both Cre(+) and day 32 was observed for *Art2b* (adenosine ribosyl transferase 2b), which could resemble the massive infiltration of T cells (Koch-Nolte et al., 1999).
As mentioned above, this study used bulk mRNA sequencing and therefore could not conclusively determine which cells caused the observed changes in purinergic molecule expression. Therefore, the effects of purinergic molecule expression at the blood-brain barrier differs depending on the cell type and may have controverse long-term effects.

First, *P2rx4* expression on microvessel components in mice exhibits contrasting effects in stroke models. Cerebral endothelial cell specific P2X4 expression exerts neuroprotection in middle cerebral artery occlusion, a common mouse model of stroke (Ozaki et al., 2016). P2X4 also protects endothelial cells by enhancing vasodilative nitric oxide production and interacting with VE-cadherin, a key protein for endothelial cell barrier integrity (Burnstock, 2016, Glass et al., 2002, Loesch, 2021). Conversely, knocking out P2X4 in myeloid immune cells provides immediate neuroprotection in early stroke phases but leads to depression-like symptoms and poorer long-term functional recovery (Srivastava et al., 2020). Additionally, astrocytes and neurons expressing P2X4 might affect vascular tone and blood-brain barrier integrity (Loesch, 2021).
Second, the upregulation of adenosine receptors has different effects on the blood-brain barrier. Activation of Adora1 and Adora2a receptors exacerbates

blood-brain barrier permeability (Wang et al., 2023, Bynoe et al., 2015), while Adora2b and Adora3 agonists may protect it (Carman et al., 2011). For instance, Adora2b agonist BAY 60-6583 reduced brain swelling and BBB disruption in ischemic stroke rats (Li et al., 2017). Similarly, the Adora3 agonist AST-004 decreased BBB permeability and neuroinflammation, enhancing spatial memory in traumatic brain injury mice (Bozdemir et al., 2021). However, the specific cellular source of these adenosine receptors remains unclear yet.

Thirdly, elevated mRNA levels of purinergic enzymes CD73 and adenosine deaminase (ADA) supposedly have anti-inflammatory effects. While ATP-rich environments promote immune cell adhesion to endothelium, adenosine inhibits it (Salmi and Jalkanen, 2005, Aslam et al., 2021). Consistent with our discoveries in BrEndO mice, a study investigating hypercholesterolemia reveals a parallel trend, wherein CD73 and ADA expression in cerebral endothelial cells exhibit a dual increase pattern (Czuba-Pakula et al., 2023). This phenomenon redirects extracellular concentration towards adenosine and inosine. CD73 degrades adenosine monophosphate (AMP) to adenosine, crucial in acute tissue protection (Thompson et al., 2004, Hart et al., 2008, Eckle et al., 2007) and repressing pro-inflammatory responses in humans (Grünewald and Ridley, 2010). Moreover, CD73 knockout mice, which lack CD73 expression on cerebral endothelial cells, showed reduced T cell infiltration into the CNS, thereby impeding the induction of experimental autoimmune encephalomyelitis (EAE), a mouse model of multiple sclerosis (Mills et al., 2008). This finding in EAE is highlighted by the beneficial effects of interferon beta, a commonly used anti-inflammatory drug for multiple sclerosis, which may also be partially attributed to the upregulation of CD73 on blood-brain barrier cells (Kiss et al., 2007).

Moreover, ADA degrades adenosine to inosine, which is then taken up by cells and further processed to uric acid (Cristalli et al., 2001). Overall, ADA activity is altered in various autoimmune conditions (Gao et al., 2021). The impact of ADA on cerebral endothelial cells is less studied. A study on children with ADA2 gene loss (CECR1) revealed a complex vascular syndrome, including strokes and endothelial integrity defects (Zhou et al., 2014). Therefore, increased ADA expression might contribute to blood-brain barrier homeostasis.

Future research should clarify the exact cellular sources of ADA and CD73 in BrEndO mice and explore cell type-specific overexpression and knockout models of P2X4, CD73, and ADA to identify possible protective therapy strategies for the blood-brain barrier integrity. Moreover, the effects of purinergic signaling appear to vary with the stage of neuroimmunological diseases. Optimal therapeutic benefits may be achieved in early stages of inflammation.

4.5 Lentiviral vectors allow overexpression or knockdown of purinergic molecules in a murine cerebral endothelial cell line

The role of purinergic molecules in cerebral endothelial cells of the blood-brain barrier is complex and not fully understood. A key research gap is replicating human-like levels of purinergic enzymes involved in ATP degradation, particularly by increasing CD73 expression while reducing CD39 and CD38 expression (Mills et al., 2011).

To address this gap, we modified the bEnd.3 cell line, an immortalized murine cerebral endothelial cell line used in neurovascular research (Qosa et al., 2016). Using lentiviral transduction, we developed three versions of these cells: one with increased CD73 expression and two with the CD39 and CD38 genes knocked out. We confirmed that the modified cells successfully overexpress CD73 and effectively degrade AMP (see section 3.3 for details).

Future experiments with these cell lines should focus on functional assays. One should investigate how these three purinergic modifications affect the cells response to ATP, AMP and NAD, or to changes in membrane potential, interactions in co-culture systems, and responses to various drugs (Li et al., 2006). These studies will help to understand how purinergic molecules function in brain endothelial cells and provide insights into conditions such as cerebral vasculitis.

5. Abstract

This thesis explores the role of purinergic signaling in experimental murine cerebral vasculitis. The focus lies on the CD8 T cell-mediated pathogenesis in the BrEndO mouse model, which is characterized by Tamoxifen-inducible ovalbumin expression in cerebral endothelial cells. Our study revealed that SIINFEKL-specific CD8 T cells infiltrate brain parenchyma during BrEndO vasculitis. Notably, in the late recovery phase, these CD8 T cells exhibit upregulation of CXCR6 and the purinergic ecto-enzyme CD39. We also found a significant upregulation of the purinergic ATP receptor P2X7 on brain infiltrating CD8 T cells. Using an inhibitory nanobody against P2X7, we observed reduced infiltration of CD8 T cells and clinical improvement of the BrEndO mice. Additionally, through bulk mRNA sequencing, we investigated purinergic molecule expression on cerebral microvessels, identifying mRNA upregulation of ATP receptor P2X4, adenosine receptors, CD73 ecto-enzyme, and adenosine deaminase. While the definite cellular source of this upregulation remains unclear, potential anti-inflammatory and protective effects on the blood-brain barrier are indicated. In conclusion, targeting purinergic molecules holds promise for addressing CD8 T cell brain infiltration and maintaining an anti-inflammatory environment at the blood-brain-barrier in BrEndO vasculitis.

6. Abstract (german)

Diese Dissertation untersucht die Rolle von purinergen Signalwegen in experimenteller muriner zerebraler Vaskulitis. Dabei liegt der Fokus auf der CD8 T-Zell-vermittelten Pathogenese im BrEndO Mausmodell, das durch die Tamoxifen-induzierte Expression von Ovalbumin in zerebralen Endothelzellen induziert wird. In dieser Arbeit wird gezeigt, dass SIINFEKL-spezifische CD8 T-Zellen im Rahmen der BrEndO Vaskulitis in das Hirnparenchym infiltrieren. Besonders in der späten Krankheitsphase weisen diese CD8 T-Zellen eine Hochregulation von CXCR6 und des purinergen Ektoenzyms CD39 auf. Darüber hinaus zeigt sich eine signifikante Hochregulation des purinergen ATP-Rezeptors P2X7 auf in das Gehirn infiltrierten CD8 T Zellen. Durch die Verwendung eines inhibierenden Nanobodies gegen P2X7 kann eine reduzierte Infiltration von CD8 T Zellen sowie klinische Verbesserungen der BrEndO Mäuse beobachtet werden. Ferner wurde mittels bulk mRNA-Sequenzierung die Expression purinerger Moleküle auf zerebralen Mikrogefäßen untersucht und auf mRNA-Level eine Hochregulation der ATP-Rezeptoren P2X4, einiger Adenosin Rezeptoren, des purinergen Ektoenzyms CD73 und der Adenosindeaminase identifiziert. Während die genaue zelluläre Quelle der beobachteten purinergen mRNA-Regulation noch unklar bleibt, gibt es Hinweise auf mögliche entzündungshemmende und protektive Effekte von purinergen Signalwegen auf die Blut-Hirn-Schranke. Zusammenfassend lässt sich sagen, dass die gezielte Beeinflussung von purinergen Signalwegen vielversprechend ist, um die Hirninfiltration von CD8 T-Zellen zu reduzieren und eine anti-inflammatorische Umgebung in experimenteller zerebraler Vaskulitis (BrEndO) zu gewährleisten.

7. Acknowledgement

First, I would like to thank my doctoral supervisor Prof. Tim Magnus, who gave me the opportunity to work in his laboratory in a great atmosphere and supported me throughout the process of my dissertation. Particular thanks go to my scientific supervisor Dr. Björn Rissiek who introduced me into a wide variety of experimental methods in his group, instructed me to work with the experimental cerebral vasculitis model and patiently reviewed my doctoral thesis. I particularly appreciate the fruitful conversations that we had about the experiments. He also gave me the opportunity to publish some results of my experimental work as a first author of a manuscript. I would also like to thank Dr. Ines Schädlich, Dr. Marco Er-Lukowiak and Joschi Stabernack for their motivating cooperation and for every laugh I shared with them. I would like to thank Lennart Kuchenbecker-Pöls for all his support in the project and many great conversations over coffee. I am very grateful that he always had an open ear for me especially when things were not always working as expected. Special thanks go to Riekje Winzer who supported me throughout the whole year and was always very optimistic to find a good solution for any problem. I am particularly grateful to Prof. Eva Tolosa who provided invaluable advice during my early scientific development. I would like to cordially thank Julia Faul and Alex Waterhölter, who always motivated me in the writing process of my thesis and were open for every discussion. Finally, I would like to thank my parents who have always motivated and inspired me throughout my life.

8. Abbreviations

ADA	adenosine deaminase
ATP	*adenosine triphosphate*
APC	*antigen presenting cells*
BrEndO	***Br**ain **End**othelial **O**valbumin vasculitis mouse model*
°C	*Degrees Celsius*
CD	*Cluster of Differentiation*
CXCR6	*C-X-C motif chemokine receptor 6*
DAMPS	*Danger Associated Molecular Patterns*
DEX	*Dextramer molecule*
EAE	*Experimental Autoimmune Encephalitis*
et al.	*et alteri*
FACS	*Fluorescence-Activated Cell Sorting*
FBS / FCS	*fetal bovine serum / fetal calve serum*
Fig.	*Figure*
FITC	*Fluorescein isothiocyanate*
g	*gram*
HA	*Hemagglutinin*
h	*hour*
IL	*Interleukin*
MFI	Mean fluorescence intensity
µg	*Microgram*
MHC	Major histocompatibility complex
min	*Minute*
µl	*Microliter*
ml	*Milliliter*
PACNS	*Primary Angiitis of the central nervous system*
PAMPS	*Pathogen associated molecular patterns*
PBS	*Phosphate buffered saline*
PE	*Phycoerythrin*
PRR	*Pattern Recognition Receptor*
qPCR	*quantitative Polymerase Chain Reaction*
rpm	*revolutions per minute*

9. References

ALLARD, B., LONGHI, M. S., ROBSON, S. C. & STAGG, J. 2017. The ectonucleotidases CD39 and CD73: Novel checkpoint inhibitor targets. *Immunol Rev,* 276**,** 121-144.

AMERSFOORT, J., EELEN, G. & CARMELIET, P. 2022. Immunomodulation by endothelial cells - partnering up with the immune system? *Nat Rev Immunol,* 22**,** 576-588.

ASLAM, M., GUNDUZ, D., TROIDL, C., HEGER, J., HAMM, C. W. & SCHULZ, R. 2021. Purinergic Regulation of Endothelial Barrier Function. *Int J Mol Sci,* 22.

BELTRAN, E., GERDES, L. A., HANSEN, J., FLIERL-HECHT, A., KREBS, S., BLUM, H., ERTL-WAGNER, B., BARKHOF, F., KUMPFEL, T., HOHLFELD, R. & DORNMAIR, K. 2019. Early adaptive immune activation detected in monozygotic twins with prodromal multiple sclerosis. *J Clin Invest,* 129**,** 4758-4768.

BERLIT, P. & KRäMER, M. 2018. S1-Leitlinie Zerebrale Vaskulitis und zerebrale Beteiligung bei systemischen Vaskulitiden und rheumatischen Grunderkrankungen. *DGNeurologie,* 1**,** 17-37.

BORGES DA SILVA, H., BEURA, L. K., WANG, H., HANSE, E. A., GORE, R., SCOTT, M. C., WALSH, D. A., BLOCK, K. E., FONSECA, R., YAN, Y., HIPPEN, K. L., BLAZAR, B. R., MASOPUST, D., KELEKAR, A., VULCHANOVA, L., HOGQUIST, K. A. & JAMESON, S. C. 2018. The purinergic receptor P2RX7 directs metabolic fitness of long-lived memory CD8(+) T cells. *Nature,* 559**,** 264-268.

BORGES DA SILVA, H., PENG, C., WANG, H., WANHAINEN, K. M., MA, C., LOPEZ, S., KHORUTS, A., ZHANG, N. & JAMESON, S. C. 2020. Sensing of ATP via the Purinergic Receptor P2RX7 Promotes CD8(+) Trm Cell Generation by Enhancing Their Sensitivity to the Cytokine TGF-beta. *Immunity,* 53**,** 158-171 e6.

BOZDEMIR, E., VIGIL, F. A., CHUN, S. H., ESPINOZA, L., BUGAY, V., KHOURY, S. M., HOLSTEIN, D. M., STOJA, A., LOZANO, D. & TUNCA, C. 2021. Neuroprotective roles of the adenosine A3 receptor agonist AST-

004 in mouse model of traumatic brain injury. *Neurotherapeutics,* 18**,** 2707-2721.

BURNSTOCK, G. 1972. Purinergic nerves. *Pharmacol Rev,* 24**,** 509-81.

BURNSTOCK, G. 2007. Physiology and pathophysiology of purinergic neurotransmission. *Physiol Rev,* 87**,** 659-797.

BURNSTOCK, G. 2016. Purinergic Signalling and Endothelium. *Curr Vasc Pharmacol,* 14**,** 130-45.

BURNSTOCK, G. 2017. Purinergic Signalling: Therapeutic Developments. *Front Pharmacol,* 8**,** 661.

BURNSTOCK, G. & KNIGHT, G. E. 2018. The potential of P2X7 receptors as a therapeutic target, including inflammation and tumour progression. *Purinergic Signal,* 14**,** 1-18.

BURNSTOCK, G. & RALEVIC, V. 1994. New insights into the local regulation of blood flow by perivascular nerves and endothelium. *Br J Plast Surg,* 47**,** 527-43.

BUSSELAAR, J., TIAN, S., VAN EENENNAAM, H. & BORST, J. 2020. Helpless Priming Sends CD8(+) T Cells on the Road to Exhaustion. *Front Immunol,* 11**,** 592569.

BYNOE, M. S., VIRET, C., YAN, A. & KIM, D. G. 2015. Adenosine receptor signaling: a key to opening the blood-brain door. *Fluids Barriers CNS,* 12**,** 20.

CAMPAGNO, K. E. & MITCHELL, C. H. 2021. The P2X(7) Receptor in Microglial Cells Modulates the Endolysosomal Axis, Autophagy, and Phagocytosis. *Front Cell Neurosci,* 15**,** 645244.

CARAMBIA, A., GOTTWICK, C., SCHWINGE, D., STEIN, S., DIGIGOW, R., SELECI, M., MUNGALPARA, D., HEINE, M., SCHURAN, F. A., CORBAN, C., LOHSE, A. W., SCHRAMM, C., HEEREN, J. & HERKEL, J. 2021. Nanoparticle-mediated targeting of autoantigen peptide to cross-presenting liver sinusoidal endothelial cells protects from CD8 T-cell-driven autoimmune cholangitis. *Immunology,* 162**,** 452-463.

CARMAN, A. J., MILLS, J. H., KRENZ, A., KIM, D. G. & BYNOE, M. S. 2011. Adenosine receptor signaling modulates permeability of the blood-brain barrier. *J Neurosci,* 31**,** 13272-80.

CEKIC, C. & LINDEN, J. 2016. Purinergic regulation of the immune system. *Nat Rev Immunol,* 16**,** 177-92.

CERTO, M., ELKAFRAWY, H., PUCINO, V., CUCCHI, D., CHEUNG, K. C. P. & MAURO, C. 2021. Endothelial cell and T-cell crosstalk: Targeting metabolism as a therapeutic approach in chronic inflammation. *Br J Pharmacol,* 178**,** 2041-2059.

CHEN, G. Y. & NUNEZ, G. 2010. Sterile inflammation: sensing and reacting to damage. *Nat Rev Immunol,* 10**,** 826-37.

CONG, L. & ZHANG, F. 2015. Genome engineering using CRISPR-Cas9 system. *Chromosomal mutagenesis***,** 197-217.

CRISTALLI, G., COSTANZI, S., LAMBERTUCCI, C., LUPIDI, G., VITTORI, S., VOLPINI, R. & CAMAIONI, E. 2001. Adenosine deaminase: functional implications and different classes of inhibitors. *Med Res Rev,* 21**,** 105-28.

CZUBA-PAKULA, E., PELIKANT-MALECKA, I., LIETZAU, G., WOJCIK, S., SMOLENSKI, R. T. & KOWIANSKI, P. 2023. Accelerated Extracellular Nucleotide Metabolism in Brain Microvascular Endothelial Cells in Experimental Hypercholesterolemia. *Cell Mol Neurobiol,* 43**,** 4245-4259.

CZUPALLA, C. J., YOUSEF, H., WYSS-CORAY, T. & BUTCHER, E. C. 2018. Collagenase-based Single Cell Isolation of Primary Murine Brain Endothelial Cells Using Flow Cytometry. *Bio Protoc,* 8.

DANQUAH, W., MEYER-SCHWESINGER, C., RISSIEK, B., PINTO, C., SERRACANT-PRAT, A., AMADI, M., IACENDA, D., KNOP, J. H., HAMMEL, A., BERGMANN, P., SCHWARZ, N., ASSUNçãO, J., ROTTHIER, W., HAAG, F., TOLOSA, E., BANNAS, P., BOUé-GRABOT, E., MAGNUS, T., LAEREMANS, T., STORTELERS, C. & KOCH-NOLTE, F. 2016. Nanobodies that block gating of the P2X7 ion channel ameliorate inflammation. *Sci Transl Med,* 8**,** 366ra162.

DE MARCHI, E., ORIOLI, E., PEGORARO, A., SANGALETTI, S., PORTARARO, P., CURTI, A., COLOMBO, M. P., DI VIRGILIO, F. & ADINOLFI, E. 2019. The P2X7 receptor modulates immune cells infiltration, ectonucleotidases expression and extracellular ATP levels in the tumor microenvironment. *Oncogene,* 38**,** 3636-3650.

DEB-CHATTERJI, M., SCHUSTER, S., HAEUSSLER, V., GERLOFF, C., THOMALLA, G. & MAGNUS, T. 2019. Primary Angiitis of the Central Nervous System: New Potential Imaging Techniques and Biomarkers in Blood and Cerebrospinal Fluid. *Front Neurol,* 10**,** 568.

DI VIRGILIO, F., DAL BEN, D., SARTI, A. C., GIULIANI, A. L. & FALZONI, S. 2017. The P2X7 Receptor in Infection and Inflammation. *Immunity,* 47**,** 15-31.

DOS SANTOS RODRIGUES, B., LAKKADWALA, S., KANEKIYO, T. & SINGH, J. 2019. Development and screening of brain-targeted lipid-based nanoparticles with enhanced cell penetration and gene delivery properties. *Int J Nanomedicine,* 14**,** 6497-6517.

DOUDNA, J. A. & CHARPENTIER, E. 2014. Genome editing. The new frontier of genome engineering with CRISPR-Cas9. *Science,* 346**,** 1258096.

DUDEK, M., PFISTER, D., DONAKONDA, S., FILPE, P., SCHNEIDER, A., LASCHINGER, M., HARTMANN, D., HüSER, N., MEISER, P., BAYERL, F., INVERSO, D., WIGGER, J., SEBODE, M., ÖLLINGER, R., RAD, R., HEGENBARTH, S., ANTON, M., GUILLOT, A., BOWMAN, A., HEIDE, D., MüLLER, F., RAMADORI, P., LEONE, V., GARCIA-CACERES, C., GRUBER, T., SEIFERT, G., KABAT, A. M., MALLM, J. P., REIDER, S., EFFENBERGER, M., ROTH, S., BILLETER, A. T., MüLLER-STICH, B., PEARCE, E. J., KOCH-NOLTE, F., KäSER, R., TILG, H., THIMME, R., BOETTLER, T., TACKE, F., DUFOUR, J. F., HALLER, D., MURRAY, P. J., HEEREN, R., ZEHN, D., BöTTCHER, J. P., HEIKENWäLDER, M. & KNOLLE, P. A. 2021. Auto-aggressive CXCR6(+) CD8 T cells cause liver immune pathology in NASH. *Nature,* 592**,** 444-449.

DUHEN, T., DUHEN, R., MONTLER, R., MOSES, J., MOUDGIL, T., DE MIRANDA, N. F., GOODALL, C. P., BLAIR, T. C., FOX, B. A., MCDERMOTT, J. E., CHANG, S. C., GRUNKEMEIER, G., LEIDNER, R., BELL, R. B. & WEINBERG, A. D. 2018. Co-expression of CD39 and CD103 identifies tumor-reactive CD8 T cells in human solid tumors. *Nat Commun,* 9**,** 2724.

ECKLE, T., KRAHN, T., GRENZ, A., KOHLER, D., MITTELBRONN, M., LEDENT, C., JACOBSON, M. A., OSSWALD, H., THOMPSON, L. F.,

UNERTL, K. & ELTZSCHIG, H. K. 2007. Cardioprotection by ecto-5'-nucleotidase (CD73) and A2B adenosine receptors. *Circulation,* 115**,** 1581-90.

EGGERS, M., RüHL, F., HAAG, F. & KOCH-NOLTE, F. 2021. Nanobodies as probes to investigate purinergic signaling. *Biochem Pharmacol,* 187**,** 114394.

EPPERSON, D. E. & POBER, J. S. 1994. Antigen-Presenting Function of Human Endothelial Cells. *J Immunol,* 153**,** 5402-5412.

FU, C. & JIANG, A. 2018. Dendritic Cells and CD8 T Cell Immunity in Tumor Microenvironment. *Front Immunol,* 9**,** 3059.

GAO, Z. W., WANG, X., ZHANG, H. Z., LIN, F., LIU, C. & DONG, K. 2021. The roles of adenosine deaminase in autoimmune diseases. *Autoimmun Rev,* 20**,** 102709.

GERASIMOVSKAYA, E. & KACZMAREK, E. 2010. *Extracellular ATP and adenosine as regulators of endothelial cell function: Implications for health and disease*, Springer Science & Business Media.

GIULIANI, A. L., SARTI, A. C. & DI VIRGILIO, F. 2020. Ectonucleotidases in Acute and Chronic Inflammation. *Front Pharmacol,* 11**,** 619458.

GLASS, R., LOESCH, A., BODIN, P. & BURNSTOCK, G. 2002. P2X4 and P2X6 receptors associate with VE-cadherin in human endothelial cells. *Cell Mol Life Sci,* 59**,** 870-81.

GONG, T., LIU, L., JIANG, W. & ZHOU, R. 2020. DAMP-sensing receptors in sterile inflammation and inflammatory diseases. *Nat Rev Immunol,* 20**,** 95-112.

GOUELI, S. A. & HSIAO, K. 2019. Monitoring and characterizing soluble and membrane-bound ectonucleotidases CD73 and CD39. *PLoS One,* 14**,** e0220094.

GRASSI, F. 2020. The P2X7 Receptor as Regulator of T Cell Development and Function. *Frontiers in Immunology,* 11.

GROSS, C. C., MEYER, C., BHATIA, U., YSHII, L., KLEFFNER, I., BAUER, J., TROSCHER, A. R., SCHULTE-MECKLENBECK, A., HERICH, S., SCHNEIDER-HOHENDORF, T., PLATE, H., KUHLMANN, T., SCHWANINGER, M., BRUCK, W., PAWLITZKI, M., LAPLAUD, D. A.,

LOUSSOUARN, D., PARRATT, J., BARNETT, M., BUCKLAND, M. E., HARDY, T. A., REDDEL, S. W., RINGELSTEIN, M., DORR, J., WILDEMANN, B., KRAEMER, M., LASSMANN, H., HOFTBERGER, R., BELTRAN, E., DORNMAIR, K., SCHWAB, N., KLOTZ, L., MEUTH, S. G., MARTIN-BLONDEL, G., WIENDL, H. & LIBLAU, R. 2019. CD8(+) T cell-mediated endotheliopathy is a targetable mechanism of neuro-inflammation in Susac syndrome. *Nat Commun,* 10**,** 5779.

GRüNEWALD, J. K. G. & RIDLEY, A. J. 2010. CD73 represses pro-inflammatory responses in human endothelial cells. *Journal of Inflammation,* 7**,** 10.

HARGADON, K. M., BRINKMAN, C. C., SHEASLEY-O'NEILL, S. L., NICHOLS, L. A., BULLOCK, T. N. & ENGELHARD, V. H. 2006. Incomplete differentiation of antigen-specific CD8 T cells in tumor-draining lymph nodes. *The Journal of Immunology,* 177**,** 6081-6090.

HART, M. L., MUCH, C., GORZOLLA, I. C., SCHITTENHELM, J., KLOOR, D., STAHL, G. L. & ELTZSCHIG, H. K. 2008. Extracellular adenosine production by ecto-5'-nucleotidase protects during murine hepatic ischemic preconditioning. *Gastroenterology,* 135**,** 1739-1750 e3.

HOGQUIST, K. A., JAMESON, S. C., HEATH, W. R., HOWARD, J. L., BEVAN, M. J. & CARBONE, F. R. 1994. T cell receptor antagonist peptides induce positive selection. *Cell,* 76**,** 17-27.

ISHIBASHI, A., SAGA, K., HISATOMI, Y., LI, Y., KANEDA, Y. & NIMURA, K. 2020. A simple method using CRISPR-Cas9 to knock-out genes in murine cancerous cell lines. *Sci Rep,* 10**,** 22345.

JANEWAY, C. A., JR. 1992. The immune system evolved to discriminate infectious nonself from noninfectious self. *Immunol Today,* 13**,** 11-6.

JANK, L., PINTO-ESPINOZA, C., DUAN, Y., KOCH-NOLTE, F., MAGNUS, T. & RISSIEK, B. 2019. Current Approaches and Future Perspectives for Nanobodies in Stroke Diagnostic and Therapy. *Antibodies (Basel),* 8.

JOOLHARZADEH, P. & ST HILAIRE, C. 2019. CD73 (Cluster of Differentiation 73) and the Differences Between Mice and Humans. *Arterioscler Thromb Vasc Biol,* 39**,** 339-348.

KIMBLE, A. L., SILVA, J., OMAR, O. M., MURPHY, M., HENSEL, J. A., NICHOLAS, S. E., JELLISON, E. R., REESE, B. & MURPHY, P. A. 2022.

A method for rapid flow-cytometric isolation of endothelial nuclei and RNA from archived frozen brain tissue. *Lab Invest,* 102**,** 204-211.

KISS, J., YEGUTKIN, G. G., KOSKINEN, K., SAVUNEN, T., JALKANEN, S. & SALMI, M. 2007. IFN-beta protects from vascular leakage via up-regulation of CD73. *Eur J Immunol,* 37**,** 3334-8.

KOCH-NOLTE, F., DUFFY, T., NISSEN, M., KAHL, S., KILLEEN, N., ABLAMUNITS, V., HAAG, F. & LEITER, E. H. 1999. A new monoclonal antibody detects a developmentally regulated mouse ecto-ADP-ribosyltransferase on T cells: subset distribution, inbred strain variation, and modulation upon T cell activation. *J Immunol,* 163**,** 6014-22.

KOIZUMI, T., KERKHOFS, D., MIZUNO, T., STEINBUSCH, H. W. M. & FOULQUIER, S. 2019. Vessel-Associated Immune Cells in Cerebrovascular Diseases: From Perivascular Macrophages to Vessel-Associated Microglia. *Front Neurosci,* 13**,** 1291.

KRAEMER, M. & BERLIT, P. 2021. Primary central nervous system vasculitis - An update on diagnosis, differential diagnosis and treatment. *J Neurol Sci,* 424**,** 117422.

LABUN, K., MONTAGUE, T. G., KRAUSE, M., TORRES CLEUREN, Y. N., TJELDNES, H. & VALEN, E. 2019. CHOPCHOP v3: expanding the CRISPR web toolbox beyond genome editing. *Nucleic Acids Res,* 47**,** W171-w174.

LAUWEREYS, M., ARBABI GHAHROUDI, M., DESMYTER, A., KINNE, J., HöLZER, W., DE GENST, E., WYNS, L. & MUYLDERMANS, S. 1998. Potent enzyme inhibitors derived from dromedary heavy-chain antibodies. *Embo j,* 17**,** 3512-20.

LEE, Y. K., UCHIDA, H., SMITH, H., ITO, A. & SANCHEZ, T. 2019. The isolation and molecular characterization of cerebral microvessels. *Nat Protoc,* 14**,** 3059-3081.

LI, Q., HAN, X., LAN, X., HONG, X., LI, Q., GAO, Y., LUO, T., YANG, Q., KOEHLER, R. C., ZHAI, Y., ZHOU, J. & WANG, J. 2017. Inhibition of tPA-induced hemorrhagic transformation involves adenosine A2b receptor activation after cerebral ischemia. *Neurobiology of Disease,* 108**,** 173-182.

LI, X., BERG, N. K., MILLS, T., ZHANG, K., ELTZSCHIG, H. K. & YUAN, X. 2020. Adenosine at the Interphase of Hypoxia and Inflammation in Lung Injury. *Front Immunol,* 11**,** 604944.

LI, X., ZHOU, T., ZHI, X., ZHAO, F., YIN, L. & ZHOU, P. 2006. Effect of hypoxia/reoxygenation on CD73 (ecto-5′-nucleotidase) in mouse microvessel endothelial cell lines. *Microvascular Research,* 72**,** 48-53.

LINDEN, J., KOCH-NOLTE, F. & DAHL, G. 2019. Purine Release, Metabolism, and Signaling in the Inflammatory Response. *Annu Rev Immunol,* 37**,** 325-347.

LOESCH, A. 2021. On P2X receptors in the brain: microvessels. Dedicated to the memory of the late Professor Geoffrey Burnstock (1929-2020). *Cell Tissue Res,* 384**,** 577-588.

LUDEWIG, P., WINNEBERGER, J. & MAGNUS, T. 2019. The cerebral endothelial cell as a key regulator of inflammatory processes in sterile inflammation. *J Neuroimmunol,* 326**,** 38-44.

MABROUK, N., TRAN, T., SAM, I., POURMIR, I., GRUEL, N., GRANIER, C., PINEAU, J., GEY, A., KOBOLD, S., FABRE, E. & TARTOUR, E. 2022. CXCR6 expressing T cells: Functions and role in the control of tumors. *Frontiers in Immunology,* 13.

MAI, J., VIRTUE, A., SHEN, J., WANG, H. & YANG, X. F. 2013. An evolving new paradigm: endothelial cells--conditional innate immune cells. *J Hematol Oncol,* 6**,** 61.

MCCARTHY, A. E., YOSHIOKA, C. & MANSOOR, S. E. 2019. Full-Length P2X(7) Structures Reveal How Palmitoylation Prevents Channel Desensitization. *Cell,* 179**,** 659-670 e13.

MENZEL, S., DUAN, Y., HAMBACH, J., ALBRECHT, B., WENDT-COUSIN, D., WINZER, R., TOLOSA, E., RISSIEK, A., GUSE, A. H., HAAG, F., MAGNUS, T., KOCH-NOLTE, F. & RISSIEK, B. 2024. Generation and characterization of antagonistic anti-human CD39 nanobodies. *Front Immunol,* 15**,** 1328306.

MENZEL, S., SCHWARZ, N., HAAG, F. & KOCH-NOLTE, F. 2018. Nanobody-Based Biologics for Modulating Purinergic Signaling in Inflammation and Immunity. *Front Pharmacol,* 9**,** 266.

MERKLER, D., VINCENTI, I., MASSON, F. & LIBLAU, R. S. 2022. Tissue-resident CD8 T cells in central nervous system inflammatory diseases: present at the crime scene and ...guilty. *Curr Opin Immunol,* 77**,** 102211.

MIHM, B., BERGMANN, M., BRUCK, W. & PROBST-COUSIN, S. 2014. The activation pattern of macrophages in giant cell (temporal) arteritis and primary angiitis of the central nervous system. *Neuropathology,* 34**,** 236-42.

MILLER, D. V., SALVARANI, C., HUNDER, G. G., BROWN, R. D., PARISI, J. E., CHRISTIANSON, T. J. & GIANNINI, C. 2009. Biopsy findings in primary angiitis of the central nervous system. *Am J Surg Pathol,* 33**,** 35-43.

MILLS, J. H., ALABANZA, L., WEKSLER, B. B., COURAUD, P. O., ROMERO, I. A. & BYNOE, M. S. 2011. Human brain endothelial cells are responsive to adenosine receptor activation. *Purinergic Signal,* 7**,** 265-73.

MILLS, J. H., THOMPSON, L. F., MUELLER, C., WAICKMAN, A. T., JALKANEN, S., NIEMELA, J., AIRAS, L. & BYNOE, M. S. 2008. CD73 is required for efficient entry of lymphocytes into the central nervous system during experimental autoimmune encephalomyelitis. *Proc Natl Acad Sci U S A,* 105**,** 9325-30.

MIX, M. R. & HARTY, J. T. 2022. Keeping T cell memories in mind. *Trends Immunol,* 43**,** 1018-1031.

MONIF, M., REID, C. A., POWELL, K. L., SMART, M. L. & WILLIAMS, D. A. 2009. The P2X7 receptor drives microglial activation and proliferation: a trophic role for P2X7R pore. *J Neurosci,* 29**,** 3781-91.

MONTESANO, R., PEPPER, M. S., MöHLE-STEINLEIN, U., RISAU, W., WAGNER, E. F. & ORCI, L. 1990. Increased proteolytic activity is responsible for the aberrant morphogenetic behavior of endothelial cells expressing the middle T oncogene. *Cell,* 62**,** 435-45.

MOON, H., NA, H. Y., CHONG, K. H. & KIM, T. J. 2006. P2X7 receptor-dependent ATP-induced shedding of CD27 in mouse lymphocytes. *Immunol Lett,* 102**,** 98-105.

MUELLER, S. N. & MACKAY, L. K. 2016. Tissue-resident memory T cells: local specialists in immune defence. *Nat Rev Immunol,* 16**,** 79-89.

MUYLDERMANS, S. 2013. Nanobodies: natural single-domain antibodies. *Annu Rev Biochem,* 82**,** 775-97.

OHTA, A. & SITKOVSKY, M. 2001. Role of G-protein-coupled adenosine receptors in downregulation of inflammation and protection from tissue damage. *Nature,* 414**,** 916-20.

OZAKI, T., MURAMATSU, R., SASAI, M., YAMAMOTO, M., KUBOTA, Y., FUJINAKA, T., YOSHIMINE, T. & YAMASHITA, T. 2016. The P2X4 receptor is required for neuroprotection via ischemic preconditioning. *Sci Rep,* 6**,** 25893.

PELEGRIN, P. 2021. P2X7 receptor and the NLRP3 inflammasome: Partners in crime. *Biochem Pharmacol,* 187**,** 114385.

PINTO, C. 2018. *Optimization of nanobodies for in vivo targeting of P2X7 ion channel on brain microglia and kidney T cells.*

QIN, D. 2019. Next-generation sequencing and its clinical application. *Cancer Biol Med,* 16**,** 4-10.

QOSA, H., MOHAMED, L. A., AL RIHANI, S. B., BATARSEH, Y. S., DUONG, Q. V., KELLER, J. N. & KADDOUMI, A. 2016. High-Throughput Screening for Identification of Blood-Brain Barrier Integrity Enhancers: A Drug Repurposing Opportunity to Rectify Vascular Amyloid Toxicity. *J Alzheimers Dis,* 53**,** 1499-516.

RACZKOWSKI, F., RISSIEK, A., RICKLEFS, I., HEISS, K., SCHUMACHER, V., WUNDENBERG, K., HAAG, F., KOCH-NOLTE, F., TOLOSA, E. & MITTRUCKER, H. W. 2018. CD39 is upregulated during activation of mouse and human T cells and attenuates the immune response to Listeria monocytogenes. *PLoS One,* 13**,** e0197151.

RIDDER, D. A., LANG, M. F., SALININ, S., RöDERER, J. P., STRUSS, M., MASER-GLUTH, C. & SCHWANINGER, M. 2011. TAK1 in brain endothelial cells mediates fever and lethargy. *J Exp Med,* 208**,** 2615-23.

RISSIEK, B., LUKOWIAK, M., HAAG, F., MAGNUS, T. & KOCH-NOLTE, F. 2018. Monitoring the Sensitivity of T Cell Populations Towards NAD(+) Released During Cell Preparation. *Methods Mol Biol,* 1813**,** 317-326.

RIVAS-YANEZ, E., BARRERA-AVALOS, C., PARRA-TELLO, B., BRICENO, P., ROSEMBLATT, M. V., SAAVEDRA-ALMARZA, J., ROSEMBLATT, M.,

ACUNA-CASTILLO, C., BONO, M. R. & SAUMA, D. 2020. P2X7 Receptor at the Crossroads of T Cell Fate. *Int J Mol Sci,* 21.

ROSEMBLATT, M. V., PARRA-TELLO, B., BRICENO, P., RIVAS-YANEZ, E., TUCER, S., SAAVEDRA-ALMARZA, J., HORMANN, P., MARTINEZ, B. A., LLADSER, A., ROSEMBLATT, M., CEKIC, C., BONO, M. R. & SAUMA, D. 2021. Ecto-5'-Nucleotidase (CD73) Regulates the Survival of CD8+ T Cells. *Front Cell Dev Biol,* 9**,** 647058.

SAFYA, H., MELLOUK, A., LEGRAND, J., LE GALL, S. M., BENBIJJA, M., KANELLOPOULOS-LANGEVIN, C., KANELLOPOULOS, J. M. & BOBE, P. 2018. Variations in Cellular Responses of Mouse T Cells to Adenosine-5'-Triphosphate Stimulation Do Not Depend on P2X7 Receptor Expression Levels but on Their Activation and Differentiation Stage. *Front Immunol,* 9**,** 360.

SALMI, M. & JALKANEN, S. 2005. Cell-surface enzymes in control of leukocyte trafficking. *Nature Reviews Immunology,* 5**,** 760-771.

SCHENK, U., WESTENDORF, A. M., RADAELLI, E., CASATI, A., FERRO, M., FUMAGALLI, M., VERDERIO, C., BUER, J., SCANZIANI, E. & GRASSI, F. 2008. Purinergic control of T cell activation by ATP released through pannexin-1 hemichannels. *Sci Signal,* 1**,** ra6.

SEMAN, M., ADRIOUCH, S., SCHEUPLEIN, F., KREBS, C., FREESE, D., GLOWACKI, G., DETERRE, P., HAAG, F. & KOCH-NOLTE, F. 2003. NAD-induced T cell death: ADP-ribosylation of cell surface proteins by ART2 activates the cytolytic P2X7 purinoceptor. *Immunity,* 19**,** 571-82.

SMITH, C. J. & SNYDER, C. M. 2021. Inhibitory Molecules PD-1, CD73 and CD39 Are Expressed by CD8(+) T Cells in a Tissue-Dependent Manner and Can Inhibit T Cell Responses to Stimulation. *Front Immunol,* 12**,** 704862.

SRIVASTAVA, P., CRONIN, C. G., SCRANTON, V. L., JACOBSON, K. A., LIANG, B. T. & VERMA, R. 2020. Neuroprotective and neuro-rehabilitative effects of acute purinergic receptor P2X4 (P2X4R) blockade after ischemic stroke. *Exp Neurol,* 329**,** 113308.

STEINBACH, K., VINCENTI, I., EGERVARI, K., KREUTZFELDT, M., VAN DER MEER, F., PAGE, N., KLIMEK, B., ROSSITTO-BORLAT, I., DI LIBERTO,

G., MUSCHAWECKH, A., WAGNER, I., HAMMAD, K., STADELMANN, C., KORN, T., HARTLEY, O., PINSCHEWER, D. D. & MERKLER, D. 2019. Brain-resident memory T cells generated early in life predispose to autoimmune disease in mice. *Sci Transl Med,* 11.

STEINGOLD, J. M. & HATFIELD, S. M. 2020. Targeting Hypoxia-A2A Adenosinergic Immunosuppression of Antitumor T Cells During Cancer Immunotherapy. *Front Immunol,* 11**,** 570041.

SU, W., SARAVIA, J., RISCH, I., RANKIN, S., GUY, C., CHAPMAN, N. M., SHI, H., SUN, Y., KC, A., LI, W., HUANG, H., LIM, S. A., HU, H., WANG, Y., LIU, D., JIAO, Y., CHEN, P. C., SOLIMAN, H., YAN, K. K., ZHANG, J., VOGEL, P., LIU, X., SERRANO, G. E., BEACH, T. G., YU, J., PENG, J. & CHI, H. 2023. CXCR6 orchestrates brain CD8(+) T cell residency and limits mouse Alzheimer's disease pathology. *Nat Immunol,* 24**,** 1735-1747.

SWANSON, K. V., DENG, M. & TING, J. P. 2019. The NLRP3 inflammasome: molecular activation and regulation to therapeutics. *Nat Rev Immunol,* 19**,** 477-489.

TAYLOR, S. R., TURNER, C. M., ELLIOTT, J. I., MCDAID, J., HEWITT, R., SMITH, J., PICKERING, M. C., WHITEHOUSE, D. L., COOK, H. T., BURNSTOCK, G., PUSEY, C. D., UNWIN, R. J. & TAM, F. W. 2009. P2X7 deficiency attenuates renal injury in experimental glomerulonephritis. *J Am Soc Nephrol,* 20**,** 1275-81.

THOMPSON, L. F., ELTZSCHIG, H. K., IBLA, J. C., VAN DE WIELE, C. J., RESTA, R., MOROTE-GARCIA, J. C. & COLGAN, S. P. 2004. Crucial role for ecto-5'-nucleotidase (CD73) in vascular leakage during hypoxia. *J Exp Med,* 200**,** 1395-405.

TIMPERI, E. & BARNABA, V. 2021. CD39 Regulation and Functions in T Cells. *International Journal of Molecular Sciences,* 22**,** 8068.

TSUDA, M., TOZAKI-SAITOH, H. & INOUE, K. 2010. Pain and purinergic signaling. *Brain Res Rev,* 63**,** 222-32.

URBAN, S. L., JENSEN, I. J., SHAN, Q., PEWE, L. L., XUE, H. H., BADOVINAC, V. P. & HARTY, J. T. 2020. Peripherally induced brain tissue-resident memory CD8(+) T cells mediate protection against CNS infection. *Nat Immunol,* 21**,** 938-949.

VARDAM-KAUR, T., VAN DIJK, S., PENG, C., WANHAINEN, K. M., JAMESON, S. C. & BORGES DA SILVA, H. 2022. The Extracellular ATP Receptor P2RX7 Imprints a Promemory Transcriptional Signature in Effector CD8(+) T Cells. *J Immunol,* 208**,** 1686-1699.

VELTKAMP, A. W., MAGNUS, T. & RISSIEK, B. 2022. Real-Time Flow Cytometry as a Tool to Monitor Cellular Consequences of P2X7 Activation in Multiple Cell Populations Mixed in a Single FACS Tube. *Methods Mol Biol,* 2510**,** 291-302.

VINCENTI, I., PAGE, N., STEINBACH, K., YERMANOS, A., LEMEILLE, S., NUNEZ, N., KREUTZFELDT, M., KLIMEK, B., DI LIBERTO, G., EGERVARI, K., PICCINNO, M., SHAMMAS, G., MARIOTTE, A., FONTA, N., LIAUDET, N., SHLESINGER, D., LIUZZI, A. R., WAGNER, I., SAADI, C., STADELMANN, C., REDDY, S., BECHER, B. & MERKLER, D. 2022. Tissue-resident memory CD8(+) T cells cooperate with CD4(+) T cells to drive compartmentalized immunopathology in the CNS. *Sci Transl Med,* 14**,** eabl6058.

VUERICH, M., MUKHERJEE, S., ROBSON, S. C. & LONGHI, M. S. 2020. Control of Gut Inflammation by Modulation of Purinergic Signaling. *Front Immunol,* 11**,** 1882.

VULTAGGIO-POMA, V. & DI VIRGILIO, F. 2022. P2 Receptors: Novel Disease Markers and Metabolic Checkpoints in Immune Cells. *Biomolecules,* 12.

WANG, Y., ZHU, Y., WANG, J., DONG, L., LIU, S., LI, S. & WU, Q. 2023. Purinergic signaling: A gatekeeper of blood-brain barrier permeation. *Front Pharmacol,* 14**,** 1112758.

WEBER, K., THOMASCHEWSKI, M., BENTEN, D. & FEHSE, B. 2012. RGB marking with lentiviral vectors for multicolor clonal cell tracking. *Nat Protoc,* 7**,** 839-49.

WEI, C., JIANG, W., WANG, R., ZHONG, H., HE, H., GAO, X., ZHONG, S., YU, F., GUO, Q., ZHANG, L., SCHIFFELERS, L. D. J., ZHOU, B., TREPEL, M., SCHMIDT, F. I., LUO, M. & SHAO, F. 2024. Brain endothelial GSDMD activation mediates inflammatory BBB breakdown. *Nature*.

WEIN, A. N., MCMASTER, S. R., TAKAMURA, S., DUNBAR, P. R., CARTWRIGHT, E. K., HAYWARD, S. L., MCMANUS, D. T., SHIMAOKA,

T., UEHA, S., TSUKUI, T., MASUMOTO, T., KURACHI, M., MATSUSHIMA, K. & KOHLMEIER, J. E. 2019. CXCR6 regulates localization of tissue-resident memory CD8 T cells to the airways. *J Exp Med,* 216**,** 2748-2762.

WIENKE, J., VELDKAMP, S. R., STRUIJF, E. M., YOUSEF YENGEJ, F. A., VAN DER WAL, M. M., VAN ROYEN-KERKHOF, A. & VAN WIJK, F. 2022. T cell interaction with activated endothelial cells primes for tissue-residency. *Front Immunol,* 13**,** 827786.

WILMES, M., PINTO ESPINOZA, C., LUDEWIG, P., STABERNACK, J., LIESZ, A., NICKE, A., GELDERBLOM, M., GERLOFF, C., FALZONI, S., TOLOSA, E., DI VIRGILIO, F., RISSIEK, B., PLESNILLA, N., KOCH-NOLTE, F. & MAGNUS, T. 2022. Blocking P2X7 by intracerebroventricular injection of P2X7-specific nanobodies reduces stroke lesions. *J Neuroinflammation,* 19**,** 256.

YUAN, X., FERRARI, D., MILLS, T., WANG, Y., CZOPIK, A., DOURSOUT, M. F., EVANS, S. E., IDZKO, M. & ELTZSCHIG, H. K. 2021. Editorial: Purinergic Signaling and Inflammation. *Front Immunol,* 12**,** 699069.

ZHOU, Q., YANG, D., OMBRELLO, A. K., ZAVIALOV, A. V., TORO, C., ZAVIALOV, A. V., STONE, D. L., CHAE, J. J., ROSENZWEIG, S. D., BISHOP, K., BARRON, K. S., KUEHN, H. S., HOFFMANN, P., NEGRO, A., TSAI, W. L., COWEN, E. W., PEI, W., MILNER, J. D., SILVIN, C., HELLER, T., CHIN, D. T., PATRONAS, N. J., BARBER, J. S., LEE, C. C., WOOD, G. M., LING, A., KELLY, S. J., KLEINER, D. E., MULLIKIN, J. C., GANSON, N. J., KONG, H. H., HAMBLETON, S., CANDOTTI, F., QUEZADO, M. M., CALVO, K. R., ALAO, H., BARHAM, B. K., JONES, A., MESCHIA, J. F., WORRALL, B. B., KASNER, S. E., RICH, S. S., GOLDBACH-MANSKY, R., ABINUN, M., CHALOM, E., GOTTE, A. C., PUNARO, M., PASCUAL, V., VERBSKY, J. W., TORGERSON, T. R., SINGER, N. G., GERSHON, T. R., OZEN, S., KARADAG, O., FLEISHER, T. A., REMMERS, E. F., BURGESS, S. M., MOIR, S. L., GADINA, M., SOOD, R., HERSHFIELD, M. S., BOEHM, M., KASTNER, D. L. & AKSENTIJEVICH, I. 2014. Early-onset stroke and vasculopathy associated with mutations in ADA2. *N Engl J Med,* 370**,** 911-20.

10. Curriculum vitae

The curriculum vitae has been removed for data protection reasons.

11. Eidesstattliche Erklärung

Ich versichere ausdrücklich, dass ich die Arbeit selbständig und ohne fremde Hilfe verfasst, andere als die von mir angegebenen Quellen und Hilfsmittel nicht benutzt und die aus den benutzten Werken wörtlich oder inhaltlich entnommenen Stellen einzeln nach Ausgabe (Auflage und Jahr des Erscheinens), Band und Seite des benutzten Werkes kenntlich gemacht habe.
Ferner versichere ich, dass ich die Dissertation bisher nicht einem Fachvertreter an einer anderen Hochschule zur Überprüfung vorgelegt oder mich anderweitig um Zulassung zur Promotion beworben habe.
Ich erkläre mich einverstanden, dass meine Dissertation vom Dekanat der Medizinischen Fakultät mit einer gängigen Software zur Erkennung von Plagiaten überprüft werden kann.

Unterschrift: